Cancer Letters 447 (2019) 115–129

Contents lists available at ScienceDirect

Cancer Letters

journal homepage: www.elsevier.com/locate/canlet

Original Articles

Pyrazinib (P3), [(*E*)-2-(2-Pyrazin-2-yl-vinyl)-phenol], a small molecule pyrazine compound enhances radiosensitivity in oesophageal adenocarcinoma

Amy M. Buckley[a], Margaret R. Dunne[a], Niamh Lynam-Lennon[a], Susan A. Kennedy[a], Aoife Cannon[a], Alison L. Reynolds[b,c], Stephen G. Maher[a], John V. Reynolds[a], Breandán N. Kennedy[c], Jacintha O'Sullivan[a,*]

[a] Department of Surgery, Trinity Translational Medicine Institute, St. James's Hospital, Trinity College Dublin, Ireland
[b] UCD School of Veterinary Medicine, Veterinary Sciences Centre, University College Dublin, Ireland
[c] UCD Conway Institute & UCD School of Biomolecular and Biomedical Science, University College Dublin, Ireland

ARTICLE INFO

Keywords:
Oesophageal cancer
Radiation
Angiogenesis
Metabolism
Inflammation

ABSTRACT

Oesophageal adenocarcinoma (OAC) is an aggressive disease with 5-year survival rates of < 20%. Only 20–30% OAC patients show a beneficial response to neoadjuvant therapy. Altered mitochondrial function is linked with radioresistance in OAC. We identified pyrazinib (P3), a pyrazine phenol small molecule drug with anti-angiogenic and anti-metabolic activity *in-vivo* in zebrafish and *in-vitro* isogenic models of OAC radioresistance. Pyrazinib (P3) significantly inhibited blood vessel development in zebrafish ($p < 0.001$). *In-vivo* in zebrafish and *in-vitro* in an isogenic model of OAC radioresistance, pyrazinib (P3) significantly reduced measures of oxidative phosphorylation and glycolysis. Pyrazinib (P3) significantly reduced the surviving fraction in OE33P; radiation-sensitive and OE33R; radiation-resistant cells following irradiation. Under hypoxic conditions pyrazinib (P3) significantly reduced OE33R cell survival following 4 Gy irradiation ($p = 0.0216$). Multiplex ELISA showed significantly higher secreted levels of 9 of 30 detected inflammatory and angiogenic factors in OE33R radioresistant cells compared to OE33P cells; IL-8, IL-4, IL-6, IL-2, IL-12p70, IL-10, MCP-1, IP-10, ICAM ($p < 0.05$). Pyrazinib (P3) significantly reduced the secretions of IL-6 ($p = 0.0006$), IL-8 ($p = 0.0488$), and IL-4 ($p = 0.0111$) in OE33R cells. Collectively, these findings support further development of pyrazinib (P3) as a novel therapeutic radiosensitiser in OAC.

1. Introduction

Oesophageal cancer is an aggressive disease and the 6th most common cause of cancer-related death, accounting for approximately 400,000 deaths annually [1]. Oesophageal cancer is classified into two histological subtypes, squamous cell carcinoma (SCC) and oesophageal adenocarcinoma (OAC) [2]. A dramatic epidemiological shift in the incidence of OAC emerged in recent years in western populations, notably OAC is now the predominant histological subtype of oesophageal cancer in both Europe and the US [2,3]. Current standard treatment regimens for OAC focus on neoadjuvant treatment with chemotherapy alone (neoCT) or in combination with radiation; neoadjuvant chemoradiation (neoCRT) for locally advanced tumours, prior to surgery [4]. Surgery is associated with increased loco-regional tumour control and neoadjuvant treatment aims to reduce tumour burden prior to surgery to improve post-operative outcome. NeoCRT in combination with surgery has been associated with higher rates of overall survival [4–6]. Unfortunately, only 20–30% of patients show a complete pathological response (pCR) to neoadjuvant treatment, meaning 70–80% of patients receive a toxic treatment with little to no therapeutic gain and a subsequent delay to surgery [7–9]. Importantly, there are currently no clinico-pathological markers available to stratify patients who will achieve a beneficial response to radiation therapy or approved radiosensitisers to enhance treatment response prior to surgery. Ionizing radiation is used to exert local tumour control in over 50% of solid cancers through the induction of double strand breaks (DSB) and cellular DNA damage [7]. Importantly, OAC sensitivity to irradiation is inversely correlated to tumour burden [10]. Resistance to radiation therapy is multifactorial and associated with a number of biological processes both within the tumour itself and the surrounding

* Corresponding author.
E-mail address: OSULLIJ4@tcd.ie (J. O'Sullivan).

https://doi.org/10.1016/j.canlet.2019.01.009
Received 1 October 2018; Received in revised form 13 November 2018; Accepted 7 January 2019

microenvironment, including dysregulated cellular energetics, angiogenesis and inflammation [11–13].

Altered energy metabolism is an emerging hallmark of cancer which plays a critical role in radioresponse [11,14], and a feature of cancer cells which was originally alluded to in 1956 by Otto Warburg [15]. Cells produce energy primarily through two interconnected pathways; glycolysis and oxidative phosphorylation which involve the catabolism of glucose to pyruvate and the production of energy from glucose via the mitochondrial tricarboxylic acid cycle, respectively [14]. Warburg reported that cancer cells preferentially use the less efficient glycolytic pathway to metabolise glucose even in the presence of oxygen, termed "aerobic glycolysis" in order to facilitate survival and rapid cellular proliferation [15]. Warburg's observations, known as the "Warburg effect", have been repeatedly confirmed but in recent years it has also become apparent that the oxidative phosphorylation pathway in the mitochondria is still largely utilised by cancer cells and is critical to the provision of intermediates for cellular biosynthesis [14]. Lynam-Lennon et al., demonstrated that radioresistant OAC cancer cells have an altered metabolic phenotype compared to isogenic radiosensitive cells [11]. Radioresistant cells have a significantly higher rate of oxidative phosphorylation whereas no significant differences are observed in glycolytic rate between the isogenic OAC cell lines [11]. Radioresistant cells also show altered mitochondrial function [11]. The excess energy consumption in the radioresistant cells limits the availability of oxygen in the tumour microenvironment to act as a radiosensitiser in the radioresistant OE33R cells. Furthermore, *ex-vivo* examination of metabolic markers in treatment-naïve patient samples found *ATP5B*, a surrogate marker of oxidative phosphorylation to be expressed at significantly higher levels in patients with a poor response to neoCRT, further highlighting elevated metabolism as a driver of the radioresistant phenotype in OAC [11]. Targeting tumour metabolism may be a novel strategy to augment radioresponse in OAC.

Angiogenesis is another hallmark of cancer which plays a critical role in radiation sensitivity, a process tightly linked with cellular metabolism [12,16,17]. Angiogenesis supplies the oxygen and glucose required to fuel the metabolic cycle. A number of chemotherapeutic agents and radiation therapy alike rely on the formation of oxygen radical species to exert their cytotoxic effects; oxygen is a potent radiosensitiser, with oxygenated cells killed more readily than hypoxic cells [17]. As oxygen is required for maximal response to radiation it is of concern that combining anti-angiogenic agents with radiation may compromise tumour vasculature and result in a more hypoxic environment with reduced sensitivity to radiation [17]. Despite this concern, anti-angiogenic agents enhance tumour response when combined with single dose radiotherapy [18–20]. Anti-angiogenic agents may enhance radio-sensitivity through normalisation of the tumour vasculature and augmentation of endothelial cell response to injury, creating a more favourable environment for response to radiation therapy [17,21]. It is also critical to understand the effect of radiation on endothelial cell function for maximising the effect of radiotherapy. Importantly, radiation-induced changes of tumour vasculature is dependent on numerous factors, such as dose, fraction, tumour location and tumour size [22]. In this study we hypothesise that phenotype-based discovery of small molecule compounds with anti-angiogenic and anti-metabolic activity, specifically targeting oxidative phosphorylation may also function as radiosensitisers in OAC.

Furthermore, OAC is an inflammatory-driven upper gastrointestinal cancer [23,24]. Inflammation plays a crucial role in treatment response in OAC [24]. Components of the complement system C3a and C4a, were shown to be higher in the pre-treatment serum of OAC patients who had a subsequent poor pathological response to neoCRT, when compared to patients having a favourable response treatment [24]. In addition, cytokines are increasingly reported to play a role in radioresistance, *e.g.* LIF and IL-6 type cytokines are linked with radioresistance in nasopharyngeal carcinoma and OAC [25,26]. Additionally, in a radioresistant oral SCC xenograft, the administration of IL-8 and IL-6 neutralising antibodies sensitised the tumours to irradiation [27]. Inflammation is tightly linked to angiogenesis, with angiogenic networks responsible for sustaining inflammation through the supply of oxygen and nutrients to the inflammatory cells [28]. Inflammation is also tightly linked to metabolism as inflammatory cells rely on metabolites generated from the metabolic cycle to maintain their function. Thus, tumour inflammation, angiogenesis and metabolism form an interdependent network which plays a crucial role in radiation resistance. Given the inflammatory driven nature of OAC, we sought to investigate the effect of pyrazinib (P3) on the inflammatory secretome in addition to its effects on two primary hallmarks of cancer, angiogenesis and dysregulated metabolism. This study aimed to phenotypically identify compounds with anti-angiogenic and anti-metabolic activity specifically targeting oxidative phosphorylation which in turn may enhance radiosensitivity in both radiosensitive and radioresistant OAC cells from a series of small molecule compounds consisting of pyrazinib (P3), a pyrazine compound, and 22 compounds of the P series. Pyrazinib (P3) was synthesised as an analogue of quininib (Q1) and in this study we sought to determine if pyrazinib or the 22 compounds of the P series could produce more potent anti-cancer activity than its parent compound quininib in OAC. Quininib is an anti-angiogenic quinoline compound which was previously discovered to produce significant anti-angiogenic activity and inhibit tumour growth both *in-vitro* and *in-vivo* respectively [29,30]. Pyrazinib (P3) produced significantly greater anti-angiogenic activity than quininib *in-vivo* in zebrafish. *In-vivo,* in zebrafish embryos, pyrazinib (P3) and two P series compounds, P2 and P4, significantly reduced oxygen consumption rate (OCR), a measure of oxidative phosphorylation, with both P2 and pyrazinib (P3) producing a simultaneous significant reduction in extracellular acidification rate (ECAR), a measure of glycolysis. *In-vitro*, in an isogenic model of OAC radioresistance, pyrazinib (P3) significantly reduced OCR and ECAR. Pyrazinib (P3) significantly reduced surviving fraction in OE33P; radiation-sensitive and OE33R; radiation-resistant cells following 2, 4 and 6 Gy irradiation fractions. Furthermore, under hypoxic conditions pyrazinib (P3) significantly reduced the surviving fraction of OE33R cells following 4 Gy irradiation. Nine of thirty detected inflammatory and angiogenic factors were secreted at significantly higher levels in OE33R radioresistant cells when compared to OE33P cells; IL-8, IL-4, IL-6, IL-2, IL-12p70, IL-10, MCP-1, IP-10 and ICAM. Pyrazinib (P3) significantly reduced the secretions of IL-6, IL-8, IL-4 and IL-13 *in-vitro* in OE33R cells. Taken together, these findings support further development of our compound pyrazinib (P3) as a novel therapeutic radiosensitiser in OAC.

2. Methods

2.1. Ethical approval

The intersegmental vessel assay screen was approved by the UCD Animal Research Ethics Committee under protocol number AREC-P-14-69 prior to commencement of this study. The zebrafish metabolic profiling assay was approved by Trinity College Dublin Animal Research Ethics Committee prior to commencement of the study.

2.2. Small molecule compounds

Quininib (Q1), pyrazinib (P3) and 22 P series compounds were synthesised by Celtic Catalysts (Ireland) and Onyx Scientific (UK). Compounds were dissolved in 100% DMSO.

2.3. Zebrafish husbandry

Tg*(fli1:*EGFP*)* zebrafish were maintained on a 14 h light/10 h dark cycle at 28 °C, in a recirculating aquaculture system, according to standard procedures [31]. Embryos were obtained through natural spawning and developmental stages were determined using time and morphological criteria [32]. Fertilised eggs were obtained from mating

adult Tg(*fli1:*EGFP) zebrafish and stored in an incubator at 28 °C. Embryos were analysed under an Olympus-SZX16 at time of collection; undeveloped-embryos were removed to prevent a delay to development of other embryos.

2.4. Intersegmental vessel assay

At 6 hours post fertilisation (hpf) Tg(*fli1:*EGFP) zebrafish embryos were plated, 5 per well in a 48-well plate, using an Olympus-SZX16 microscope in 400 µl embryo medium (EM) (5 mM NaCl, 0.17 mM KCl, 0.4 mM $CaCl_2$ and 0.16 mM $MgSO_4$). EM was removed and 400 µl containing EM and control or test compound was added to each well. 100 µM solutions, dissolved in dH_2O/1% DMSO of Q1, pyrazinib (P3) and 22 P series compounds were stored at −20ºC. Compounds were defrosted to room temperature (RT) and vortexed before use. Drug treatments were carried out in duplicate and repeated three times at 10 µM. Treated larvae were incubated until 48 hpf at 28 °C on a 14 h light/10 h dark cycle.

After incubation, larvae were placed in 400 µl of phosphate-buffered-saline (PBS) and dechorionated under an Olympus-SZX16 microscope. Larvae were euthanized and fixed in 400 µl of 4% para-formaldehyde (PFA) in a paraffilm-covered plate at RT for 2 h. 400 µl of PFA was removed and larvae were washed three times at 10 min intervals with 400 µl PBS. Larvae were stored in 400 µl of PBS in a paraffin-covered 48-well plate at 4 °C until analysis.

2.5. Quantification of intersegmental vessels

Prior to analysis of intersegmental vasculature, larvae were screened using an Olympus-SZX16 microscope for morphological defects. Larvae were placed on a depression slide on their side with their head in a left pointing orientation. Anti-angiogenic activity was determined on the basis of (a) the total inhibition of intersegmental vessel (ISV) growth and (b) incomplete sprouting of the intersegmental vessel (ISV) from the dorsal aorta (DA) to the dorsal longitudinal anastomatic vessel (DLAV). Intersegmental vasculature was viewed by epi-fluorescence under an Olympus SZX16 microscope using a green fluorescent protein (GFP) filter. The number of complete intersegmental vessels was quantified for each sample and larvae were imaged using cell^F software (Olympus, Europe).

2.6. Zebrafish metabolic profiling assay

26 hpf Tg(*fli1:*EGFP) zebrafish embryos were plated, 3 per well in a 24-well islet cell microplate (Agilent Technologies, Santa Clara, CA, USA), using an Olympus-SZX16 microscope in 700 µl EM containing a final concentration of 10 µM of test compounds; Q1, pyrazinib (P3), P2, P4, P18, P20, P8 and P23 or 0.1% DMSO as control, with 5 wells per treatment group. Four wells contained EM only to identify temperature fluctuations across the plate. Drug treated larvae were incubated for 24 h at 28 °C on a 14 h light/10 h dark cycle until 50 hpf. At 50 hpf, an islet screen (Agilent Technologies, Santa Clara, CA, USA) was inserted above the embryos in each well to prevent the embryos contacting the sensor probe during the course of the assay. The Seahorse XFe24 analyser (Agilent Technologies, Santa Clara, CA, USA) couples a sensor cartridge with a custom cell plate. Sensor probes which are close to the islet screen sense changes and measure the levels of dissolved oxygen and free protons in this microchamber at indicated intervals, giving a read-out of Oxygen Consumption Rate (OCR) and Extracellular Acidification rate (ECAR), a measure of oxidative phosphorylation and glycolysis, respectively. Prior to the assay the XFe24 cartridge plate (Agilent Technologies, Santa Clara, CA, USA) was hydrated overnight in a 37 °C non-CO_2 incubator. At 50 hpf three measurements were taken over 24 min consisting of three repeats of mix (3 min)/wait (2 min)/measurement (3 min) to establish basal respiration. Upon completion of assay, larvae were euthanized and fixed in 400 µl of 4% PFA in a paraffilm-covered plate at RT for 2 h.

2.7. Generation of the OE33P and OE33R cell lines

The human OE33 oesophageal adenocarcinoma cell line was obtained from the European Collection of Authenticated Cell Cultures. The isogenic model of radioresistant OAC; OE33P (radiosensitive) and OE33R (radioresistant) cells was generated as previously described [33].

2.8. OCR and ECAR measurements in OE33P and OE33R cells

OE33P and OE33R cells were seeded in triplicate at a density of 11,000 and 13,000 cells/well, respectively in 24-well cell culture XFe24 microplates (Agilent Technologies, Santa Clara, CA, USA) at a volume of 100 µl and allowed to adhere at 37 °C in 5% CO_2/95% air. 5 h later, an additional 150 µl/well complete cell culture Roswell Park Memorial Institute medium (RPMI) 1640 medium was added. 24 h later, OE33P and OE33R cells were treated with 10 µM of Q1, pyrazinib (P3), P2, P4, P18, P20, P8 and P23 or 0.1% DMSO control. Following 24 h treatment, media was removed and cells were washed with unbuffered Dulbecco's Modified Eagle's medium (DMEM) supplemented with 10 mM glucose (Sigma-Aldrich) and 10 mM sodium pyruvate (Sigma Aldrich), (pH 7.4) and incubated for 1 h at 37 °C in a CO_2-free incubator. OCR and ECAR were measured using a Seahorse Biosciences XFe24 Extracellular Flux Analyser (Agilent Technologies, Santa Clara, CA, USA). Three basal measurements of OCR and ECAR were taken over 24 min consisting of three repeats of mix (3 min)/wait (2 min)/measurement (3 min) to establish basal respiration. Three additional measurements were obtained over 24 min each following the injection of 3 mitochondrial inhibitors including oligomycin (2 µg·mL−1,Sigma Aldrich), an uncoupling agent Carbonyl cyanide 4-(trifluoromethoxy) phenylhydrazone (FCCP) (5 µM, Sigma Aldrich) and antimycin-A (2 µM, Sigma Adrich). ATP turnover was calculated by subtracting the OCR post oligomycin injection from baseline OCR prior to oligomycin addition. Maximal respiration was calculated by subtracting OCR post antimycin A addition from OCR post FCCP addition. Spare respiratory capacity was calculated by subtracting basal OCR from maximal respiration. All measurements were normalised to cell number using the crystal violet assay, transferring the eluted stain to a 96-well plate before reading.

2.9. Crystal violet

Cells were fixed with 1% glutaraldehyde (Sigma-Aldrich) for 15 min at RT. The fixative was removed and cells were washed with PBS and stained with 0.1% crystal violet in PBS for 30 min at RT. Plates were left to air dry and incubated with 50 µl 1% Triton X-100 in PBS on a plate shaker for 30 min at RT. Absorbance was read at 595 nm on a VersaMax microplate reader (Molecular Devices, Sunnyvale, CA, USA).

2.10. ROS levels

Reactive oxygen species levels were measured using 2,7-dichlorofluorescein (DCF) which emits a fluorescent signal linearly linked to the intracellular H_2O_2. OE33P and OE33R cells were seeded at a density of 8,000 cells/well in triplicate and allowed to adhere overnight. 24 h after seeding, OE33P and OE33R cells were treated for 24 h with µ µ0.1% DMSO control or 10 µM Q1, pyrazinib (P3), P2, P4, P18, P20, P8 and P23 in RPMI. 24 h later media was removed from wells. 50 µl of 5 µM 2,7-DCF (Invitrogen, Carlsbad, CA, USA) in PBS Mg^{++} (Sigma-Aldrich) was added to each well and incubated for 30 min at 37 °C in 5% CO_2/95% air. The probe was removed and 100 µl PBS was added to each well, fluorescence was measured FLx800 Fluorescence Microplate Reader (Mason Technology Dublin, Ireland). Fluorescence was normalised to cell number using the crystal violet assay, as previously described.

2.11. Mitochondrial membrane potential

To assess mitochondrial membrane potential, the fluorescent probe rhodamine 123 (5 μM), which is selectively taken up by mitochondria and its uptake dependent on mitochondrial membrane potential was used. OE33P and OE33R cells were seeded at a density of 8,000 cells/well in triplicate and allowed to adhere overnight. 24 h later, OE33P and OE33R cells were treated with 0.1% DMSO or 10 μM of Q1, pyrazinib (P3), P2, P4, P18, P20, P8 and P23 for 24 h. 24 h later, the media was removed from wells and cells were washed with 100 μl of PBS. 50 μl of 5 μM rhodamine 123 in PBS Mg^{++} solution was added to each well and incubated for 30 min at 37 °C in 5% CO_2/95% air. The probe was removed and 100 μl of PBS added to each well. Fluorescence was measured on FLx800 Fluorescence Microplate Reader (Mason Technology Dublin, Ireland). Fluorescence was normalised to cell number using the crystal violet assay, as previously described.

2.12. Mitochondrial mass

MitoTracker Green (0.3 μM, Invitrogen, Carlsbad, CA, USA), a mitochondrial selective dye was used to evaluate mitochondrial mass in OE33P and OE33R cells treated with 10 μM of our compounds. OE33P and OE33R cells were seeded at a density of 8,000 cells/well in triplicate in 100 μl complete RPMI and allowed to adhere overnight. 24 h later after seeding, OE33P and OE33R cells were treated with 0.1% DMSO or 10 μM Q1, pyrazinib (P3), P2, P4, P18, P20, P8 and P23. 24 h later media was removed and 50 μl of 0.3 μM MitoTracker Green in PBS Mg^{++} and incubated for 30 min at 37 °C in 5% CO_2/95% air. The probe was removed and 100 μl PBS was added to each well and fluorescence was measured on FLx800 Fluorescence Microplate Reader (Mason Technology Dublin, Ireland). Fluorescence was normalised to cell number using the crystal violet assay, as previously described.

2.13. Clonogenic assay

OE33P and OE33R cells were trypsinised, counted and seeded at the optimised densities of 1–11 × 10^3 in 1.5 ml complete RPMI in triplicate in 6 well plates and allowed to adhere overnight. 24 h later OE33P and OE33R cells were treated with 0.1% DMSO or 10 μM of Q1, pyrazinib (P3), P2 and P4. 24 h later OE33P and OE33R cells were either irradiated at 2, 4 or 6 Gy or mock irradiated. OE33P and OE33R cells were additionally treated with either 0.1% DMSO or pyrazinib at 1, 5 or 10 μM for 24 h or 10 μM for 72 h prior to irradiation. Colonies were allowed to grow for 7–14 days at which point they were fixed and stained with 0.05% crystal violet (25% methanol in dH_2O) and allowed to air dry. Clonogenics carried out under hypoxic conditions were seeded and allowed to adhere at 37 °C in 5% CO_2/95% air for 6 h before being transferred to the Whitley H35 hypoxy-station at 37 °C in 5%CO_2/0.5%O_2. Following 24 h incubation under hypoxic conditions (0.5% O_2) OE33P and OE33R cells were maintained at 0.5% O_2 and treated with 0.1% DMSO or 10 μM of pyrazinib (P3), and irradiated 24 h later at 5%CO_2/0.5%O_2. 24 h following irradiation, plates were returned to 37 °C in 5%CO_2/95% air. Colonies were allowed to grow for 7–14 days, at which point they were fixed and stained with 0.05% crystal violet and allowed to air dry. Colonies consisting of 50 cells or more were counted using a colony counter (ColCountTM, Oxford Optronix, Oxford, UK). Plating efficiency (PE), fraction of colonies formed by untreated cells, was calculated using the formula: PE = No. colonies/No. cells seeded. The surviving fraction (SF), the number of colonies formed was expressed in terms of PE, was calculated using the formula: SF = No. colonies/(No. cells seeded x PE).

2.14. Irradiation

Irradiation was performed using a Gulmay Medical X-ray generator, (RS225) (Gulmay Medical), at a dose rate of 3.25 Gray (Gy) per min.

2.15. Multiplex enzyme linked immunosorbent assay (ELISA)

Supernatants from OE33R and OE33P cells were defrosted on ice. The secretion of cytokines and angiogenic and inflammatory growth factors was analysed by ELISA as per the manufacturer's instructions. To assess angiogenic, vascular injury, inflammatory cytokine and chemokine secretions, a 54 multiplex kit spread across 7 plates was used (Meso Scale Diagnostics, USA). The 54 multiplex kit was used to quantify the secretions of CRP, Eotaxin, Eotaxin-3, FGF (basic), GM-CSF, ICAM-1, IFN-γ, IL-10, IL-12/IL-23p40, IL-12p70, IL-13, IL-15, IL-16, IL-17A, IL-17A/F, IL-17B, IL-17C, IL-17D, IL-1RA, IL-1α, IL-1β, IL-2, IL-21, IL-22, IL-23, IL-27, IL-3, IL-31, IL-4, IL-5, IL-6, IL-7, IL-8, IL-8 (HA), IL-9, IP-10, MCP-1, MCP-4, MDC, MIP-1α, MIP-1β, MIP-3α, PlGF, SAA, TARC, Tie-2, TNF-α, TNF-β, TSLP, VCAM-1, VEGF-A, VEGF-C, VEGF-D and VEGFR-1/Flt-1 from OE33P and OE33R cell supernatants previously treated with 10 μM pyrazinib (P3) or vehicle control (0.1% DMSO) for 24 h. Secretion data for all factors was normalised appropriately to cell lysate protein content using the BCA assay (Pierce) as per manufacteurs instructions. Data was analysed using MSD Discovery Workbench software version 4.0.

2.16. BrdU ELISA

Proliferation was assessed using the BrdU cell proliferation ELISA (Roche Diagnostics, Sussex, UK) as per manufactures instructions. Cells were seeded in triplicate at a density of 5,000 cells/ well in 96-well plates and allowed to adhere overnight, followed by treatment with 0.1% DMSO control or 10 μM Q1, pyrazinib (P3), P2, P4, P18, P20 , P8 and P23 for 24 or 72 h. 10 μM BrdU Labelling Solution was added to each well (except for background control wells) and cells were incubated for 1 h at 37°C in 5% CO_2/95% air. ELISA was carried out as per manufactures instructions and absorbance was measured at 450nm on a VersaMax microplate reader (Molecular Devices, Sunnyvale, CA, USA).

2.17. RNA isolation

Cells were seeded at a density of 2.5 × 10^5 cells/well in 6-well plates and allowed to adhere overnight. Following drug treatment with 10 μM of pyrazinib (P3) or 0.1% DMSO control for 24 h, RNA was isolated from cell lines using the TRI Reagent® method. The RNA pellet was re-suspended in 30 μl RNAase free molecular grade H_20 and stored at −80 °C.

2.18. RNA quantification

RNA quantification was determined spectrophotometrically, using a Nanodrop 1000 spectrophotometer (version 3.1.0, Nanodrop technologies, DE, USA). 1 μl RNase-free water was used to blank the instrument prior to RNA analysis. 1 μl of each sample of isolated RNA was loaded onto the instrument and concentration was measured in ng/μl.

2.19. cDNA synthesis

For cell line samples, total RNA (1 μg total RNA) was reverse transcribed to cDNA using the following method. To anneal the primers to the RNA, the sample was heated for 10 min at 70 °C, and immediately chilled for at least 1 min at 4 °C. A master mix containing RNaseOUT (Invitrogen, Carlsbad, CA, USA) recombinant ribonuclease inhibitor (1unit/μl), dNTPs (Invitrogen, Carlsbad, CA, USA) (10 mM, prepared as a 1:1:1:1 ratio of dATP, dGTP, dTTP and dCTP), Bioscript reverse transcriptase (200units/μl) (Bioline, Kilkenny, Ireland) and 5X Bioscript Reaction Buffer (Bioline, Kilkenny, Ireland) in RNase-free water was added to each sample. Samples were incubated for 1 h at 37 °C then 10 min at 70 °C and held at 4 °C. The resulting cDNA was stored at −20 °C.

2.20. Quantitative real time PCR and analysis

qPCR was performed using TaqMan primer probes (*MLH1, SMUG1, PARP1, MMS19* (Roche)) and a Quant Studio 5 real-time thermal cycler (Thermo Fisher Scientific). 18S (Applied Biosystems) was used as an endogenous control for data normalization. Data analysis was performed using Thermofisher Scientific Connect qPCR application software.

2.21. Statistical analysis

Statistical analysis was performed using GraphPad Prism version 5 software (GraphPad Software, CA, USA). Scientific data were expressed as mean ± standard error of the mean (SEM). SEM was calculated as the standard deviation of the original samples divided by the square root of the sample size. Specific statistical tests used are indicated in figure legends. For all statistical analysis, differences were considered statistically significant at $p < 0.05$.

3. Results

3.1. Pyrazinib (P3) and P series compounds inhibit developmental angiogenesis in Tg(fli1:EGFP) zebrafish

Using Tg(*fli1*:EGFP) embryos, pyrazinib (P3) & P series compounds were screened for anti-angiogenic activity in a phenotype-based approach using the intersegmental vessel assay illustrated in Fig. 1A. Compounds were tested at 10 μM and their anti-angiogenic activity assessed by quantification of intersegmental vessel number at 48 hpf (Fig. 1B). This screen was carried out to identify if pyrazinib (P3) and 22 P series compounds (Table 1) produced greater anti-angiogenic activity compared to quinoline series compound quininib (Q1) from which pyrazinib (P3) was derived. Quininib (Q1) has previously been shown to inhibit both ocular and tumour angiogenesis *in-vitro* and *in-vivo* [29,30]. A dose response profile was conducted at 1, 5 and 10 μM, with the most potent anti-angiogenic effect seen at 10 μM (data for 1 & 5 μM not shown). Pyrazinib (P3) and P series compounds P2, P4, P18 and P20 produced the most potent anti-angiogenic activity ($p < 0.0001$) compared to vehicle control. The most potent anti-angiogenic compound pyrazinib (P3), reduced ISV number by ~67% at 10 μM, whereas the quinoline compound quininib (Q1) produced a reduction in ISV number of ~35% in this screen. Furthermore, the P series compounds, pyrazinib (P3) and P4 produced significantly greater anti-angiogenic activity when compared directly to the quinoline compound quininib (Q1) when tested at 10 μM (Fig. 1B). Fluorescent images (Fig. 1C) illustrate the potent reduction in ISV number and loss of vessel integrity following treatment with pyrazinib (P3) (white arrows indicate incomplete sprouting and absence of vessel growth) and P series compounds (P2, P4, P18, P20), compared to control and quinoline series compound quininib (Q1). No gross morphological defects or toxicities were observed following treatment with pyrazinib (P3) or any other P series compounds tested in this assay, whilst there were some alterations to skin pigmentation following treatment (Fig. 1C).

Based on this ranking of pyrazinib (P3) and 22 P series compounds, it was decided to further test P series compounds which produced significant (P2, P4, pyrazinib (P3), P18 and P20) or no (P8 and P23) anti-angiogenic activity *in-vivo* to determine if these compounds could also inhibit metabolism, in particular oxidative phosphorylation metabolism, which is strongly associated with radioresistance in OAC.

3.2. Pyrazinib (P3) inhibits metabolism in Tg(fli1:EGFP) zebrafish

Using Tg(*fli1*:EGFP) embryos, pyrazinib (P3), 6 P series compounds and quininib (Q1) of the quinoline series were screened for anti-metabolic activity as illustrated in Fig. 2A. 26 hpf embryos were treated with 10 μM of test compound and anti-metabolic activity assessed at 50 hpf using the XFe24 Seahorse analyser. Pyrazinib (P3), P2 and P4 significantly reduced oxygen consumption rate (OCR) ($p = 0.0076$, $p = 0.0088$ and $p = 0.0194$ respectively), a measure of oxidative phosphorylation, producing a reduction of between ~16% and 18%

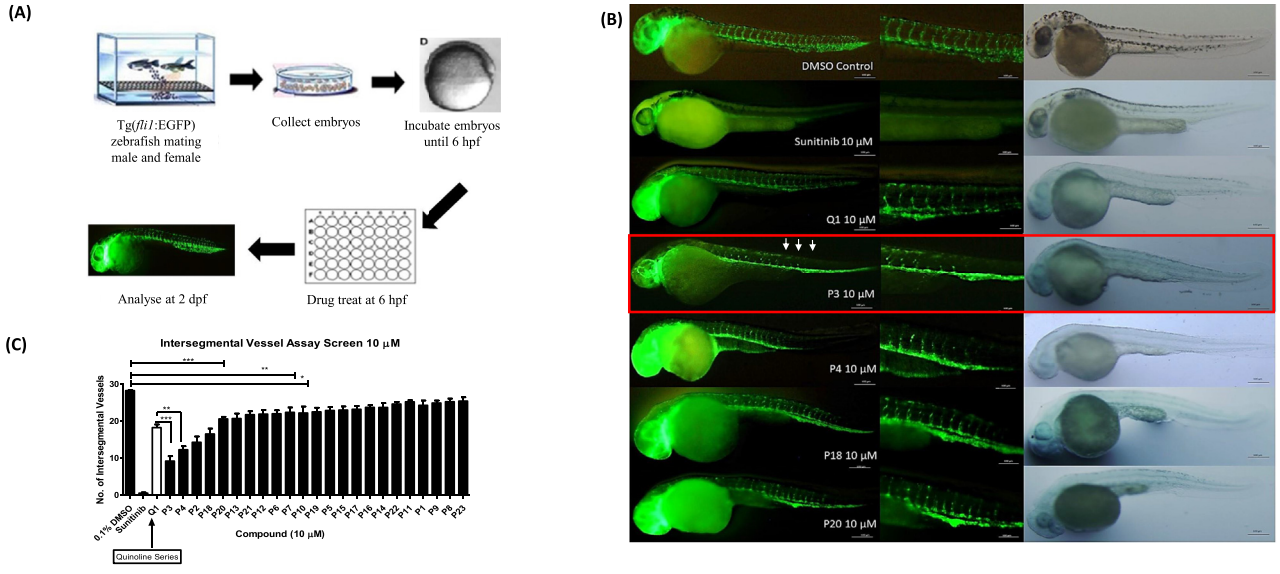

Fig. 1. Pyrazinib (P3) and P series compounds inhibit developmental angiogenesis in Tg(*fli1*:EGFP) zebrafish. (A) Intersegmental vessel assay schematic; 6 hours post fertilisation (hpf) Tg(*fli1:EGFP*) embryos were treated with compounds and fixed and analysed at 2 days post fertilisation (dpf) **(B)** Inhibition of intersegmental vasculature growth in Tg(*fli1*:EGFP) zebrafish. 6 hpf embryos were treated with 0.1% DMSO Control, sunitinib 10 μM, quininib (Q1), pyrazinib (P3) and 22 P series compounds at 10 μM as indicated on graph. Number of intersegmental vessels was quantified at 2 dpf. One-way ANOVA with Tukey post-tests ($n = 3$). Data expressed as mean + SEM; *$p < 0.05$, **$p < 0.01$ and ***$p < 0.001$. **(C)** Representative fluorescent images illustrating GFP-positive intersegmental vessels at low and high magnification and brightfield images of whole larvae at 2 dpf in Tg(*fli1*:EGFP) zebrafish treated with 0.1% DMSO Control, sunitinib, quininib (Q1), pyrazinib (P3), P2, P4, P18 and P20.

Table 1
Structures of P Series Compounds Table listing differences in chemical structures of P series compounds indicating where modifications were made to groups C2-C6, R1-R2, A, X and Y to yield P series of compounds.

Compound	Compound Chemical Name	A	C2	C3	C4	C5	C6	X	Y	R1	R2	Salt	Chemical Structure Skeleton
P1	(*E*)-2-(2-Pyridin-2-yl-vinyl)-phenol	–	N	–	–			alkene		OH			
P2	(*E*)-2-(2-Pyridin-2-yl-vinyl)-phenol HCl salt	–	N	–	–			alkene		OH		HCl	
P3	(*E*)-2-(2-Pyrazin-2-yl-vinyl)-phenol	–	N	–	–	N		alkene		OH			
P4	(*E*)-2-(2-Pyrazin-2-yl-vinyl)-phenol HCl salt	–	N	–	–	N		alkene		OH		HCl	
P5	(*E*)-2-(2-pyridin-4-yl-vinyl)-phenol	–	–	–	N			alkene		OH			
P6	(*E*)-2-(2-pyridin-4-yl-vinyl)-phenol HCl salt	–	–	–	N			alkene		OH		HCl	
P7	(*E*)-2-[2-(6-Methyl-pyridin-2-yl)-vinyl]-phenol	Me	N	–	–			alkene		OH			
P8	(*E*)-2-[2-(6-Methyl-pyridin-2-yl)-vinyl]-phenol HCl salt	Me	N	–	–			alkene		OH		HCl	
P9	(*E*)-2-(2-(pyridin-3-yl)vinyl)phenol	–	–	N	–			alkene		OH			
P10	(*E*)-2-(2-(pyridin-3-yl)vinyl)phenol hydrochloride	–	–	N	–			alkene		OH		HCl	
P11	(*E*)-2-(2-Pyraxin-2-yl-propenyl)-phenol	–	N	–	–	N		alkene	Me	OH			
P12	(*E*)-2-(2-Pyraxin-2-yl-propenyl)-phenol HCl salt	–	N	–	–	N		alkene	Me	OH		HCl	
P13	(*E*)-4-Methyl-2-(2-pyrazin-2-yl-yl-vinyl)-phenol	–	N	–	–	N		alkene		OH	Me		
P14	(*E*)-4-Methyl-2-(2-pyrazin-2-yl-yl-vinyl)-phenol HCl salt	–	N	–	–	N		alkene		OH	Me	HCl	
P15	(*E*)-2-(2-Pyrimidin-2-yl-vinyl)-phenol HCl salt	–	N	–	–		N	alkene		OH		HCl	
P16	(*E*)-2-(2-Pyridin-2-yl-vinyl)-pyrazine HCl salt	–	N	–	–	N		alkene		C=N		HCl	
P17	(*E*)-2-(2-Pyrazin-2-yl-vinyl)-benzamide HCl salt	–	N	–	–	N		alkene		CON2		HCl	
P18	2-[2-(Pyrazin-2-yl)ethynyl]phenol	–	N	–	–	N		alkyne		OH			
P19	2-[2-(2-Methoxyphenyl) ethynyl]pyrazine	–	N	–	–	N		alkyne		Ome			
P20	2-[2-(Pyrazin-2-yl)ethynyl]phenol hydrochloride	–	N	–	–	N		alkyne		OH		HCl	
P21	(*Z*)-2-[2-(Pyrazin-2-yl)vinyl]phenol	–	N	–	–	N		z-alkene		OH			
P22	(*E*)-2-(2-(IH-imidazol-2-yl)vinyl)phenol	–	N	–	–	N	–	alkene		OH			
P23	(*E*)-2-(2-(IH-imidazol-2-yl)vinyl)phenol hydrochloride	–	N	–	–	N	–	alkene		OH		HCl	

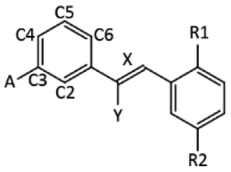

(Fig. 2B), with both pyrazinib (P3) and P2 producing a simultaneous and significant reduction in extracellular acidification rate (ECAR), a measure of glycolysis, pyrazinib (P3) ($p = 0.0059$) and P2 ($p = 0.0352$) (Fig. 2C). This significant reduction of both OCR and ECAR following treatment with 10 μM of pyrazinib (P3) and P2 illustrates the ability of these P series compounds to target the two major metabolic pathways, oxidative phosphorylation and glycolysis. In summary, *in-vivo* in zebrafish we identified three compounds of the P series; pyrazinib (P3), P2 and P4 which inhibit both angiogenesis and metabolism a significant finding given the well reported role of angiogenesis and metabolism, particularly oxidative phosphorylation in radioresponse in OAC.

3.3. Pyrazinib (P3) significantly alters metabolic rates in OE33P (radiation-sensitive) and OE33R (radiation-resistant) isogenic OAC cells

To investigate if pyrazinib (P3) and P series compounds could also induce a reduction in oxidative phosphorylation and glycolysis when tested in an *in-vitro* model, we used an isogenic OAC cell line model of radioresistance, OE33P; radiationsensitive and OE33R; radioresistant cells, which was previously generated in our laboratory [33]. The effect of our compounds on two major metabolic pathways; oxidative phosphorylation and glycolysis was assessed using the Seahorse XFe24 analyser. Following 24 h treatment of OE33P and OE33R cells with our compounds, simultaneous measurements of OCR and ECAR were recorded in live cells. Radioresistant OE33R cells produced a significantly higher OCR at baseline when compared to OE33P cells ($p < 0.05$) (Fig. 3A) but no significant difference in ECAR was observed (Fig. 3D). 24 h treatment with pyrazinib (P3) significantly reduced OCR in OE33P and OE33R cells ($p = 0.0262$, $p = 0.0044$) (Fig. 3B and C), with a simultaneous reduction in ECAR in OE33R cells ($p = 0.0162$) (Fig. 3F). Treatment with P2 produced a reduction in OCR alone in OE33R cells ($p = 0.0169$). Interestingly, the non-antiangiogenic analogue P23 increased OCR in OE33P cells (Fig. 3B) and quininib (Q1) significantly reduced ECAR in OE33P cells only (Fig. 3E). No significant effect was seen following treatment with P4, the HCl salt of pyrazinib (P3), which was previously shown to have anti-angiogenic and anti-metabolic activity in zebrafish embryos in Figs. 1B and 2B. This screen demonstrated the novel anti-cancer action of pyrazinib (P3) in its ability to produce anti-metabolic activity *in-vitro* through the production of a significant reduction in OCR in both OE33P and OE33R cells and ECAR in OE33R cells only. P series compounds; P8 and P23 which produced no effect on angiogenesis or metabolism *in-vivo* in zebrafish embryos also produced no anti-metabolic activity when tested *in-vitro* in the isogenic OAC model (Fig. 3B and C,E,F). Furthermore, ATP turnover was significantly higher in OE33R cells compared to OE33P cells ($p = 0.0260$) and treatment with pyrazinib (P3) significantly reduced ATP turnover in OE33R cells ($p = 0.0168$) (Fig. 3 G). No differences were seen in maximal respiration and spare respiratory capacity between the two cell lines or following treatment with pyrazinib (P3) (Fig. 3H, I). In summary, pyrazinib (P3) a small molecule compound significantly inhibited oxidative phosphorylation in radiation-sensitive (OE33P) and radiation-resistant (OE33R) OAC cells and produced a simultaneous reduction in glycolysis in radiation-resistant OE33R cells.

3.4. Pyrazinib (P3) reduced ROS levels in radiation-sensitive OE33P cells with no effect on mitochondrial mass and mitochondrial membrane potential

Treatment with pyrazinib (P3) and P2 was previously shown to reduce metabolic rate in the isogenic model of OAC, thus, we wanted to investigate if this reduction in metabolic rate was accompanied by changes in mitochondrial function following treatment with our compounds.

To investigate if treatment with our P series compounds induced changes in mitochondrial function we assessed alterations in reactive oxygen species (ROS) levels, mitochondrial membrane potential and mitochondrial mass, three surrogate markers of mitochondrial function. OE33R cells were associated with significantly higher basal levels of ROS ($p = 0.0151$) when compared to age and passage matched OE33P cells (Fig. 4A). Treatment with our P series compounds had a notable effect on ROS production in OE33P cells (Fig. 4B) but no changes in ROS were observed following treatment in OE33R cells (Fig. 4C). 24 h treatment with pyrazinib (P3), P2 and P18, P20 significantly reduced ROS levels in OE33P cells ($p < 0.01$) with P4, P8 and P23 also inducing a modest but significant reduction in ROS levels ($p < 0.05$) in radiation-sensitive OE33P cells (Fig. 4B). There were no significant differences in the other two surrogate markers of mitochondrial function; mitochondrial membrane potential and mitochondrial mass either between the two cell lines at baseline or following treatment with 10 μM of P series compounds (Fig. 4D–I). In summary, the potent anti-metabolic activity of pyrazinib (P3) in OE33R cells is independent of

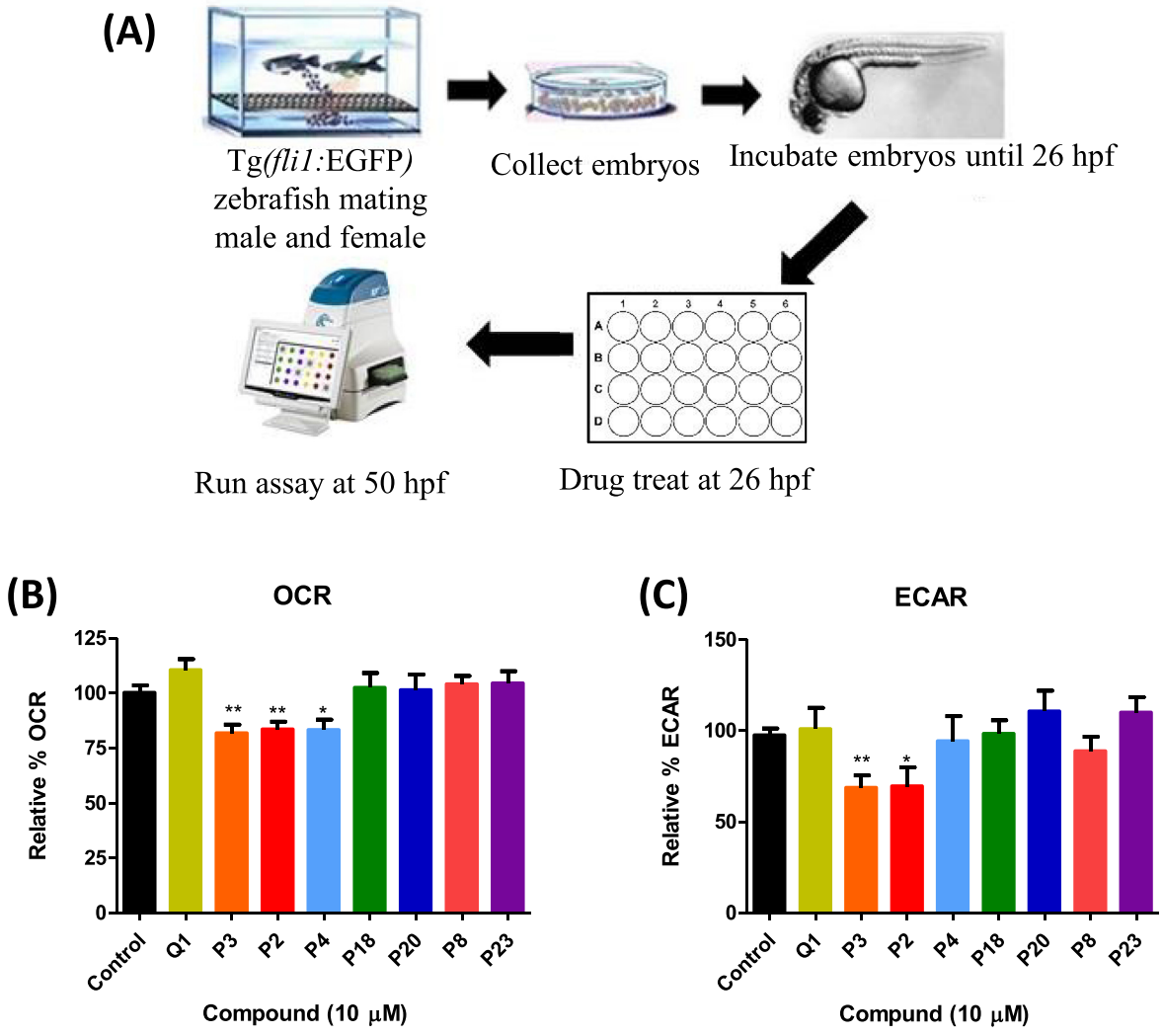

Fig. 2. Pyrazinib (P3) and P series analogues inhibit metabolism in Tg*(fli1:EGFP)* zebrafish.(A) Schematic of zebrafish real-time metabolic profiling assay; 26 hours post fertilisation (hpf) embryos were treated with P series compounds and metabolic profile was analysed at 50 hpf using the XFe24 Seahorse Biosciences analyser. **(B)** 26 hpf embryos were treated with 0.1% DMSO as control or 10 μM of P series compounds; quininib (Q1), pyrazinib (P3), P2, P4, P18, P20, P8 or P23, at 50 hpf basal OCR measurements were taken using Seahorse Biosciences XFe24 Analyser, (n = 5). **(C)** 26 hpf zebrafish embryos were treated with 0.1% DMSO or 10 μM of quininib (Q1), pyrazinib (P3), P2, P4, P18, P20, P8 and P23, at 50 hpf basal ECAR measurements using Seahorse Biosciences XFe24 Analyser, (n = 5). Data expressed as mean + SEM; Unpaired *t*-test. *p < 0.05, **p < 0.01.

changes to mitochondrial function including ROS production, mitochondrial membrane potential and mitochondrial mass.

3.5. Pyrazinib (P3) significantly enhanced radiosensitivity in-vitro in an isogenic model of oesophageal adenocarcinoma

Angiogenesis and metabolism are interconnected processes, tightly linked to the radioresistant phenotype [11,34]. We investigated the ability of our small molecule compounds with anti-angiogenic and anti-oxidative phosphorylation activity, pyrazinib (P3) and other P series compounds (P2, P4), to sensitise OAC cells to radiation. We carried out a clonogenic assay, the gold standard for assessing radiosensitivity [35]. Following 24 h treatment with 10 μM of quininib (Q1), pyrazinib (P3), P2 and P4 OE33P and OE33R cells were either irradiated (2 Gy) or mock irradiated (0 Gy). We also tested other P series compounds which had previously been shown to be anti-angiogenic and have no anti-metabolic activity; P18 and P20 and two compounds which were neither anti-angiogenic or anti-metabolic; P8 and P23 (data not shown).

Quininib (Q1), which produced significant anti-angiogenic activity and a modest but significant reduction in ECAR in OE33P cells had no effect on the surviving fraction in either cell line (Fig. 5 B, F) indicating that targeting OCR as opposed to ECAR may be more important to overcome radioresistance in OAC cells. Notably, pyrazinib (P3), which produced the most potent anti-angiogenic activity *in-vivo* in zebrafish embryos and significant anti-metabolic activity both *in-vivo* and *in-vitro,* could significantly reduce the surviving fraction in both radiation-sensitive ($p = 0.0395$) and radiation-resistant cells ($p = 0.0342$) (Fig. 5C, G). In addition, P4, the HCl salt of pyrazinib (P3), which was previously shown to have potent anti-angiogenic and anti-metabolic activity *in-vivo* produced a significant reduction in surviving fraction in both OE33P ($p = 0.0373$) and OEE3R cells ($p = 0.0220$) (Fig. 5 E, J). P2, a HCl salt which has a similar but distinctly different IUPAC structure from pyrazinib (P3) and P4, significantly reduced surviving fraction in OE33P cells ($p = 0.0246$) (Fig. 5D) and showed a trend, although not significant, towards a reduction in surviving fraction in the radio-resistant line (Fig. 5H). This result indicated that small molecule compounds which were previously shown to inhibit angiogenesis *in-vivo* and inhibit oxidative phosphorylation either *in-vivo* or *in-vitro* or both could radiosensitise OAC cells to radiation, whereas compounds which were anti-angiogenic but do not inhibit OCR, a measure of oxidative

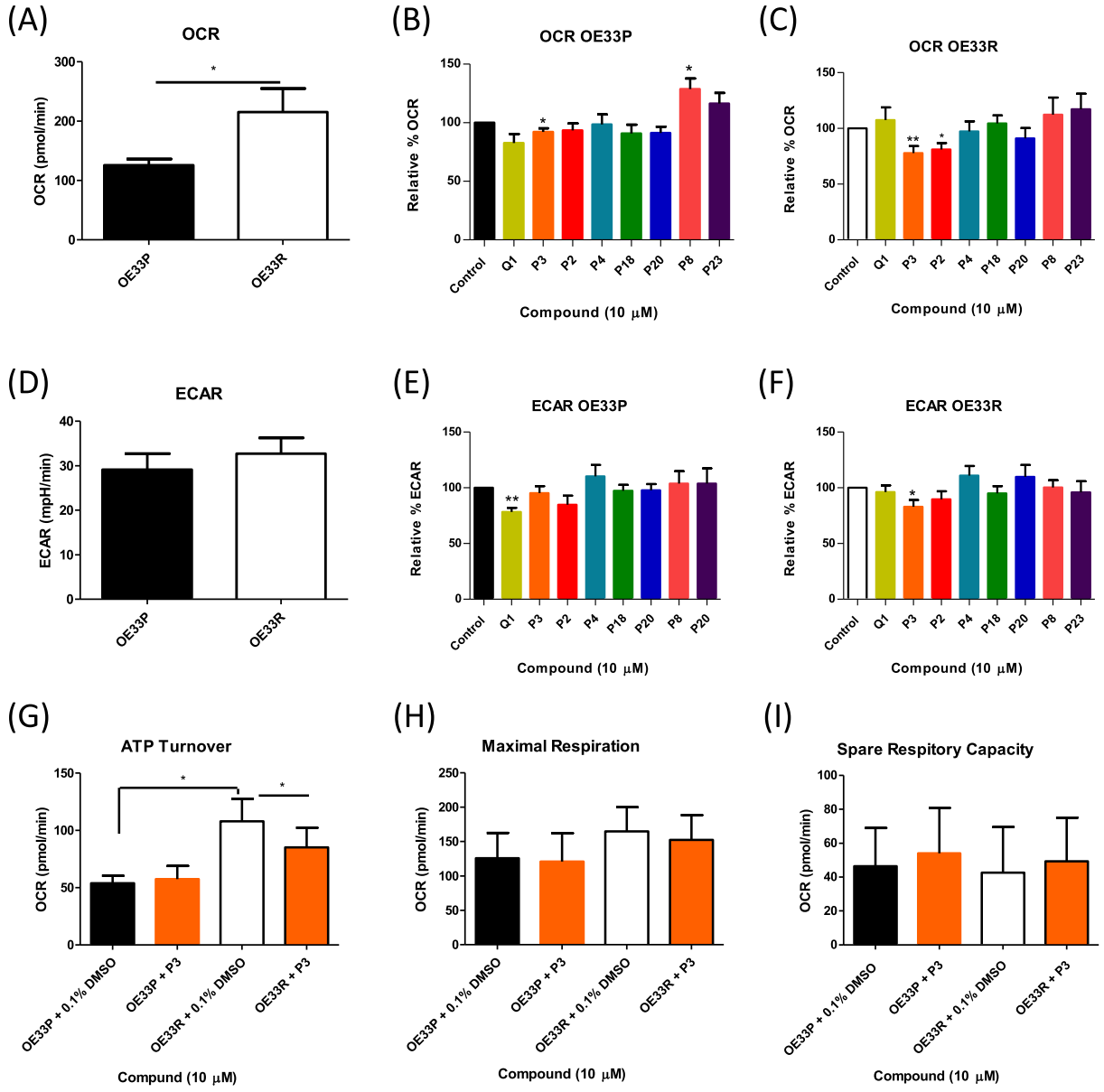

Fig. 3. Pyrazinib (P3) treatment reduced oxidative phosphorylation and glycolysis in OE33R; radioresistant OAC cells. (A) Oxygen consumption rate (OCR), a measure of oxidative phosphorylation was evaluated in OE33P and OE33R cells using the Seahorse Biosciences XFe24 analyser. OE33R cells have a significantly higher OCR when compared to OE33P; radiation sensitive cells, two-tailed unpaired *t*-test, *p < 0.05, (n = 13). **(B)** Relative percentage OCR in OE33P cells following treatment with 0.1% DMSO control or P series compounds, (n = 7, except P3 n = 12). **(C)** Percentage relative OCR in OE33R cells following treatment with 0.1% DMSO control or novel compounds at 10 μM, (n = 7, except P3 n = 12). **(D)** Extracellular acidification rate (ECAR), a measure glycolysis was evaluated in OE33P and OE33R cells using the Seahorse Biosciences XFe24 extracellular flux analyser, (n = 7, except P3 n = 12). **(E)** Relative percentage ECAR in OE33P cells following treatment with control or 10 μM of quininib (Q1), Pyrazinib (P3), P2, P4, P18, P20, P8 and P23 (n = 7, except P3 n = 12). **(F)** Pyrazinib (P3) produced a significant reduction in relative percentage ECAR in OE33R cells (n = 7 except P3 n = 12). **(G)** ATP turnover in OE33P and OE33R cells following treatment with 0.1% DSMO or pyrazinib (P3), (n = 6). **(H)** Spare Respiratory capacity in OE33P cells and OE33R cells following treatment with 0.1% DMSO or pyrazinib (P3), (n = 6). **(I)** Maximal respiration in OE33P cells and OE33R cells following treatment with 0.1% DMSO or pyrazinib (P3), (n = 6). Data are expressed as mean + SEM. Statistical analysis was carried out using an unpaired *t*-test to compare different cell lines and paired *t*-test to compare within the same cell line. Data was normalised to cell number, as assessed by crystal violet assay. *p < 0.05,**p < 0.01. (For interpretation of the references to color in this figure legend, the reader is referred to the Web version of this article.)

phosphorylation (Q1, P18 and P20) could not induce this effect nor could compounds P8 and P23, which had neither anti-angiogenic or anti-metabolic activity (data not shown). Notably, treatment with 10 μM of pyrazinib for 24 h prior to radiation was found to be the optimal dose and treatment schedule to enhance radiosensitivity in OE33P and OE33R cells (Fig. 5C,G), (Supplemental Figure 2 A-D).

3.6. Pyrazinib (P3) enhanced radiosensitivity in-vitro in an isogenic model of oesophageal adenocarcinoma at 2, 4 and 6 Gy X-ray radiation

To further investigate the ability of pyrazinib (P3) to enhance radiosensitivity in OAC we evaluated the ability of pyrazinib (P3) to radio-sensitise OE33P and OE33R cells to radiation therapy at increasing doses of radiation by clonogenic assay. As previously shown pyrazinib (P3) enhanced radiosensitivity in OE33P and OE33R cells ($p = 0.0043$, $p = 0.0051$ respectively) following 2 Gy irradiation

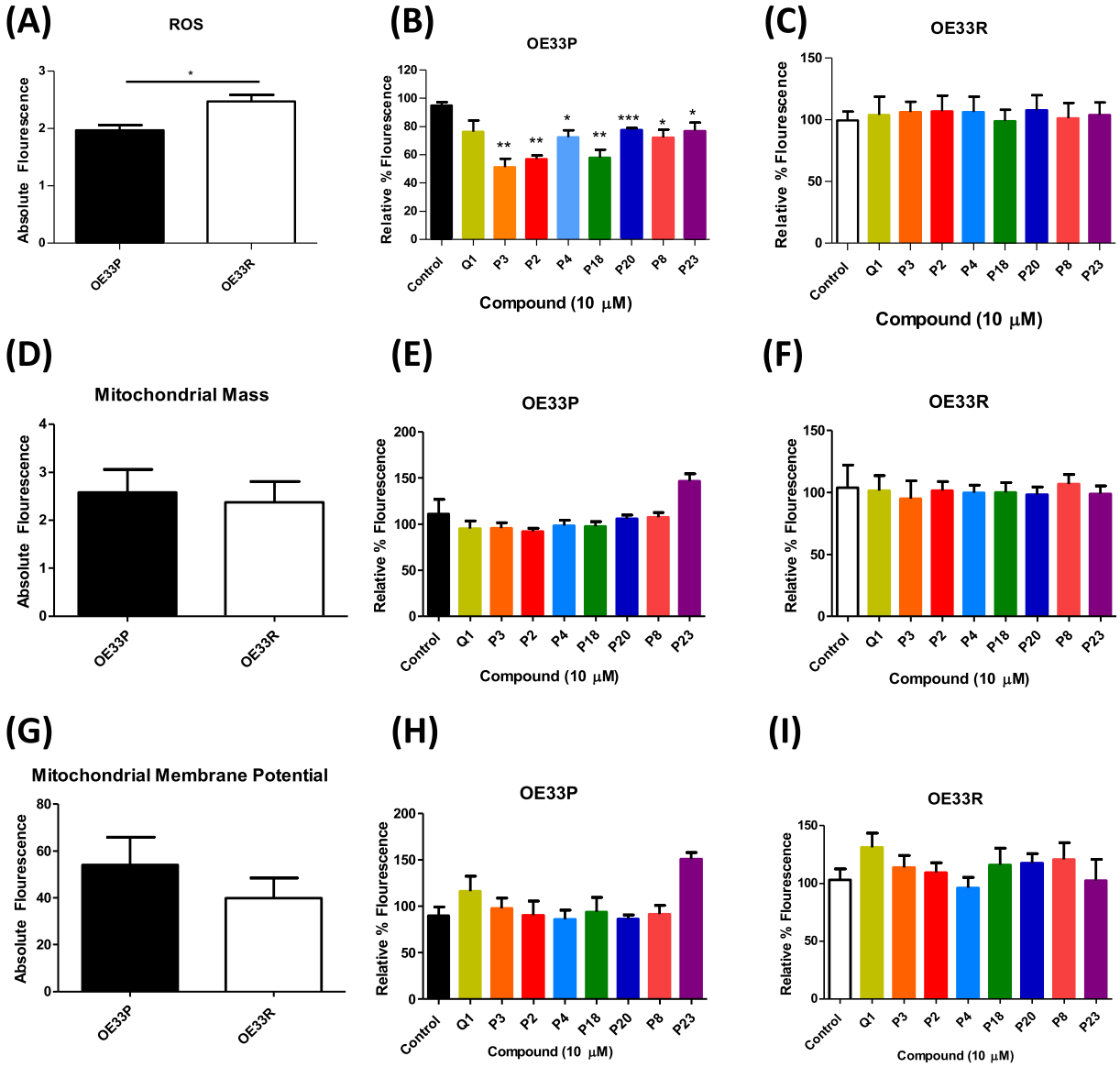

Fig. 4. Pyrazinib (P3) and P series compounds reduced ROS levels in the radiation sensitive OE33P cells with no effect on mitochondrial mass and mitochondrial membrane potential. **(A)** ROS levels are significantly higher in radiation resistant OE33R cells compared to OE33P; radiation sensitive cells, two-tailed unpaired *t*-test, (n = 4) *p < 0.05. **(B)** 24 h treatment with pyrazinib (P3) and additional P series compounds significantly reduced ROS in OE33P cells, (n = 4). **(C)** Pyrazinib (P3) and other P series compounds tested had no effect on ROS levels in OE33R cells following treatment at 10 μM, (n = 4). **(D)** Mitochondrial mass does not differ significantly between OE33P and OE33R cells, two tailed unpaired *t*-test, (n = 4) **(E)** 24 h treatment with 10 μM of P series compounds had no effect on mitochondrial mass in OE33P cells, (n = 4) **(F)** 24 h treatment with 10 μM of P series compounds did not alter mitochondrial mass in OE33R cells, (n = 4) **(G)** Mitochondrial membrane potential does not differ significantly between OE33P and OE33R cells, unpaired *t*-test, (n = 4) **(H)** 24 h treatment with 10 μM of P series compounds had no effect on mitochondrial membrane potential in OE33P cells, (n = 4) **(I)** 24 h treatment with 10 μM of P series compounds had no effect on mitochondrial membrane potential in OE33R cells, (n = 4). Statistical analysis was carried out using an unpaired *t*-test to compare different cell lines and paired *t*-test to compare within same cell line. Data was normalised to cell number, determined by crystal violet assay. Data are expressed as mean + SEM; *p < 0.05, **p < 0.01, ***p < 0.001. (For interpretation of the references to color in this figure legend, the reader is referred to the Web version of this article.)

(Fig. 6 A, B). In addition, pyrazinib (P3) enhanced radiosensitivity following irradiation at 4 Gy in OE33P (p = 0.0081) and OE33R cells (p = 0.0139) and 6 Gy in OE33P and OE33R cells (p = 0.0093, p = 0.0141 respectively).

3.7. Pyrazinib (P3) enhanced radiosensitivity in-vitro in an isogenic model of oesophageal adenocarcinoma under hypoxic conditions

Hypoxic tumours are inherently radioresistant, thus we investigated the ability of pyrazinib (P3) to enhance radiosensitivity in an environment of low oxygen (0.5% O_2). Both OE33P and OE33R cells were significantly more radioresistant to both 2 and 4 Gy radiation when cultured under hypoxic conditions (0.5% O_2) when compared to matched cells cultured under normoxic conditions (Fig. 7 A, B). Pyrazinib (P3) significantly enhanced radiosensitivity of OE33R cells cultured under hypoxic conditions following 4 Gy irradiation (Fig. 7 D) (p = 0.0216). Pyrazinib (P3) did not alter the radiosensitivity of OE33P cells cultured under hypoxic conditions of 0.5% O_2 but could enhance radiosensitivity under normoxic conditions following 2 and 4 Gy irradiation similar to results previously shown (Fig. 7C).

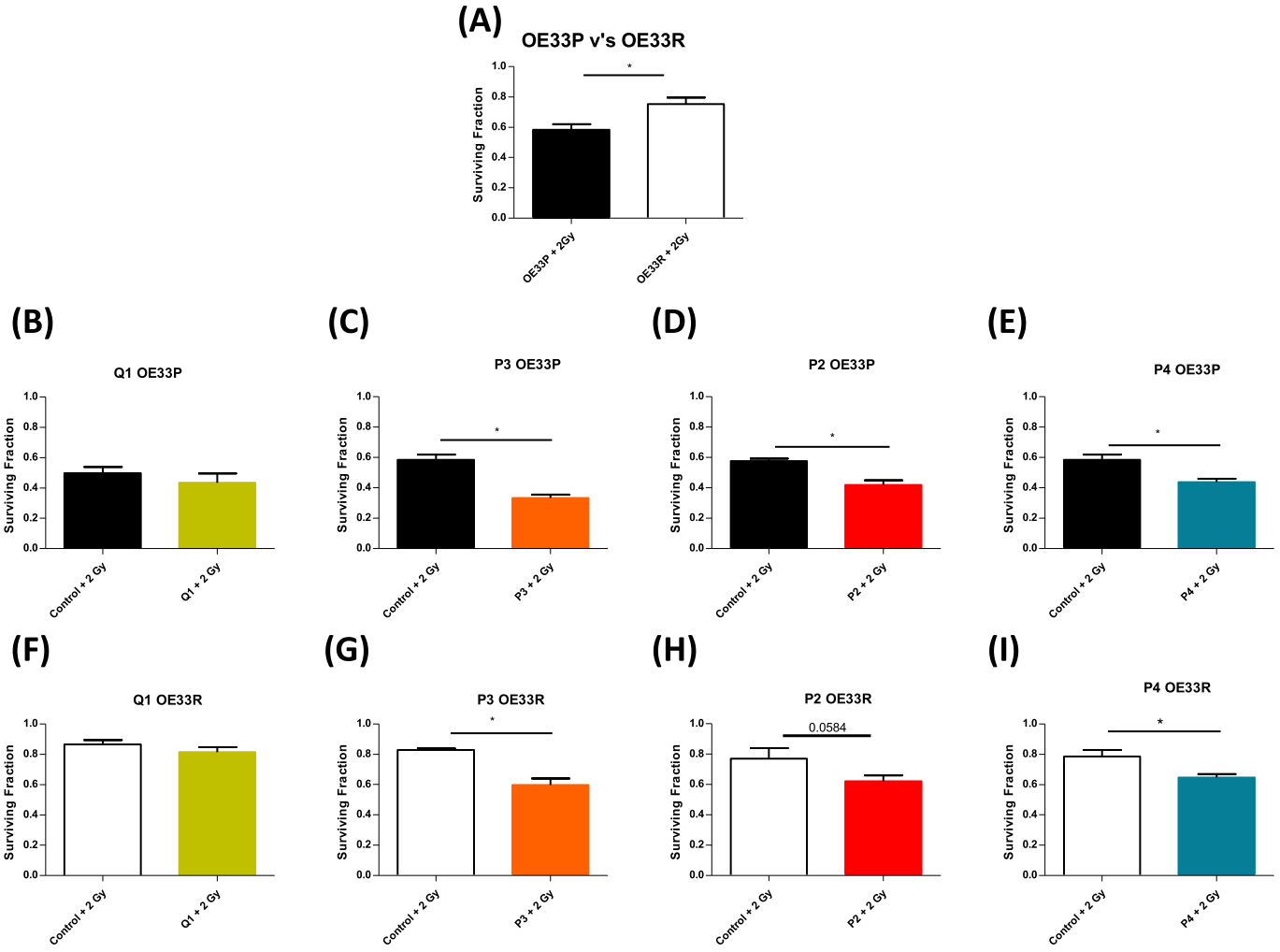

Fig. 5. Pyrazinib (P3), P2 and P4 enhanced radiosensitivity *in-vitro* in an isogenic model of Oesophageal Adenocarcinoma. The effect of 24 h treatment with P series compounds on radiosensitivity *in-vitro* was assessed by clonogenic assay. **(A)** Surviving fraction of OE33P and OE33R cells following 2 Gy radiation, OE33R radioresistant cells have a significantly higher surviving fraction when compared to OE33P radiation sensitive cells, (n = 3), unpaired *t*-test, *p < 0.05. **(B)** Surviving fraction of OE33P cells following treatment with quininib; Q1 + 2 Gy, (n = 3). **(C)** Surviving fraction of OE33P cells following treatment with pyrazinib (P3) + 2 Gy, (n = 3). **(D)** Surviving fraction of OE33P cells following treatment with P2 + 2 Gy, (n = 3) **(E)** Surviving fraction of OE33P cells following treatment with P4 + 2 Gy, (n = 3). **(F)** Surviving fraction of OE33R cells following treatment with quininib; Q1 + 2 Gy, (n = 3). **(G)** Surviving fraction of OE33R cells following treatment with pyrazinib (P3) + 2 Gy, (n = 3) **(H)** Surviving fraction of OE33R cells following treatment with P2 + 2 Gy, (n = 4). **(I)** Surviving fraction of OE33R cells following treatment with P4 + 2 Gy, (n = 4). Statistical analysis by two-tailed unpaired *t*-test to compare different cell lines and paired *t*-test to compare within same cell line. *p < 0.05. Data expressed as mean + SEM.

3.8. Pyrazinib (P3) significantly alters the secretion of IL-6, IL-4, IL-8 and IL-13 in OE33R radioresistant cells

Inflammation has previously been shown to be a negative regulator of response to radiation treatment in OAC [23,24]. We sought to investigate the difference in inflammatory protein secretions from our OE33P and OE33R cells and evaluate the effect of treatment with our radiosensitiser pyrazinib (P3) on inflammatory protein secretions in our isogenic model. We measured the effects of pyrazinib (P3) on the protein secretions of 54 angiogenic factors, growth factors and inflammatory cytokines in OE33P and OE33R cells following treatment with 10 μM pyrazinib (P3) or vehicle control. Of the 54 factors analysed, 30 were detected within the range of detection in our isogenic radioresistant OAC model. Of the 30 factors detected, 9 factors were secreted at significantly higher levels in OE33R radioresistant cells when compared to OE33P cells; IL-6, IL-4, IL-8, ICAM, IL-12p70, IL-2, IL-10, IP-10 and MCP-1 (Fig. 8A–J). Pyrazinib (P3) significantly reduced the secretions of IL-6 (p = 0.0006) (Fig. 8A), IL-4 (p = 0.0111) (Fig. 8B), IL-8 (p = 0.0488) (Fig. 8C) and IL-13 (p = 0.0204) (Fig. 8 D) *in-vitro* in OE33R cells.

4. Discussion

To date, through phenotype-based screens we have identified 3 novel small molecule compounds (pyrazinib (P3), P2 and P4) with significant anti-angiogenic and anti-metabolic activity *in-vitro* and *in-vivo,* which enhanced radiosensitivity in our isogenic model of OAC radioresistance. Pyrazinib (P3) was selected as our lead compound which significantly enhanced radiosensitivity in our isogenic model of OAC radioresistance, and was associated with significant anti-angiogenic, anti-metabolic and anti-inflammatory actions *in-vivo* in zebrafish and *in-vitro* in our isogenic model of OAC radioresistance. Importantly pyrazinib (P3) produced significantly greater anti-angiogenic and anti-metabolic activity, specifically in terms of targeting oxidative phosphorylation than its parent compound quininib, and was associated with novel radiosensitising activity in an isogenic model of OAC radioresistance.

Two of twenty-three of our P series compounds tested; pyrazinib

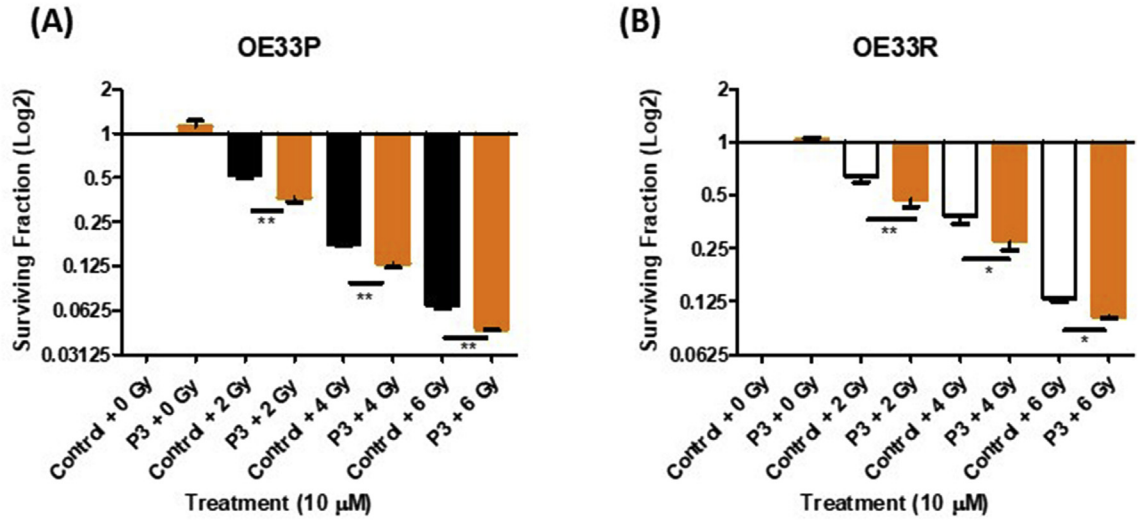

Fig. 6. Pyrazinib (P3) enhanced radiosensitivity *in-vitro* in an isogenic model of Oesophageal Adenocarcinoma at increasing fractionated doses of irradiation. The effect of treatment with pyrazinib (P3) on radiosensitivity *in-vitro* was assessed by clonogenic assay. **(A)** Surviving fraction of OE33P cells following treatment with 0.1% DMSO control or 10 μM pyrazinib (P3) and 0, 2, 4 and 6 Gy radiation, (n = 3), paired *t*-test, **p < 0.01. **(B)** Surviving fraction of OE33R cells following treatment with 0.1% DMSO control or 10 μM pyrazinib (P3) and 0, 2, 4 and 6 Gy radiation, (n = 3), paired *t*-test, *p < 0.05, **p < 0.01. Data expressed as mean + SEM.

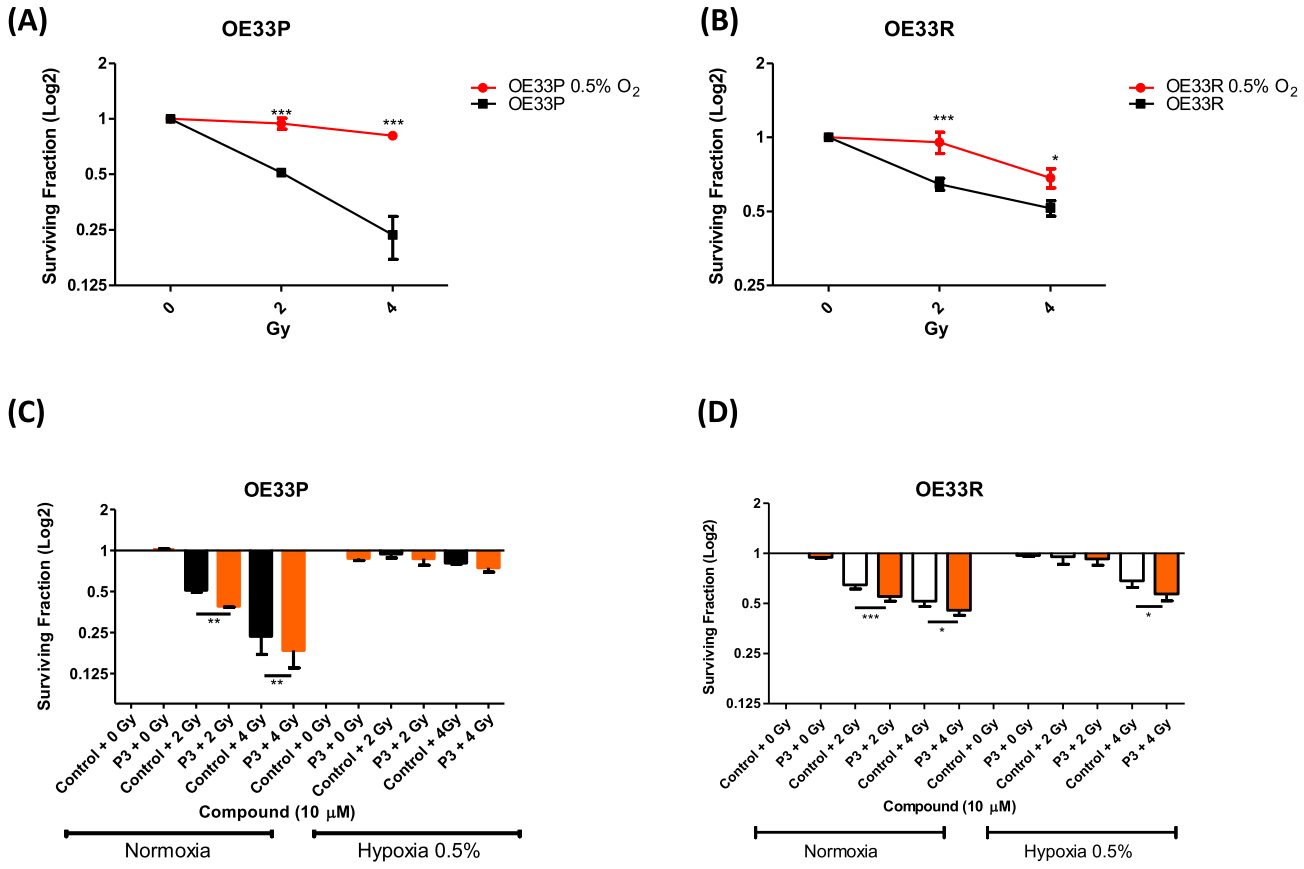

Fig. 7. Pyrazinib (P3) significantly enhanced radiosensitivity under hypoxic conditions (0.5% O_2) in OE33R; OAC radioresistant cells. The ability of pyrazinib (P3) to enhance radiosensitivity was evaluated by clonogenic assay under normoxic and hypoxic (0.5% O_2) conditions using the Whitley h35 hypoxia chamber **(A)** Surviving fraction of OE33P cells cultured under normoxic and hypoxic conditions following 0, 2 and 4 Gy irradiation, (n = 3). **(B)** Surviving fraction of OE33R cells cultured under normoxic and hypoxic conditions following 0, 2 and 4 Gy irradiation, (n = 3). **(C)** Surviving fraction of OE33P cells cultured under normoxia and hypoxia following treatment with 0.1% DMSO control or 10 μM pyrazinib (P3) and 0, 2, and 4 Gy irradiation, (n = 3). **(D)** Surviving fraction of OE33R cells cultured under normoxia or hypoxia following treatment with 0.1% DMSO control or 10 μM pyrazinib (P3) and 0, 2, and 4 Gy irradiation, (n = 3). Unpaired t-test to was used to compare differenct cell lines and paired *t*-test was used to compare within same cell line, *p < 0.05, **p < 0.01, ***p < 0.001. Data expressed as ± SEM.

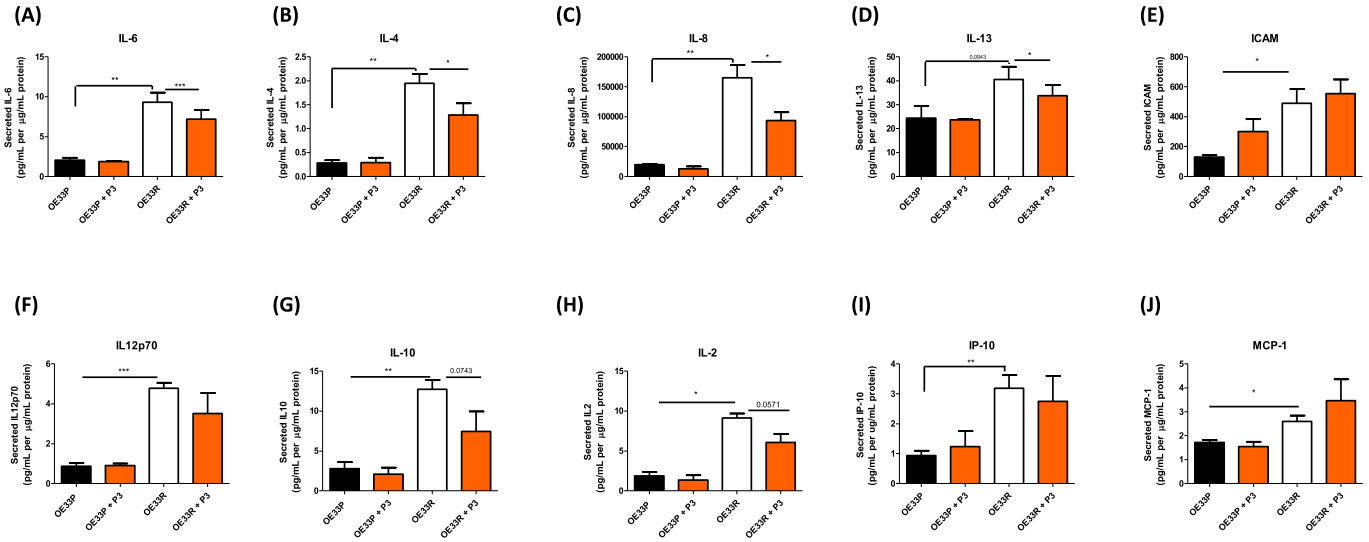

Fig. 8. Pyrazinib (P3) significantly reduced the secretion of IL-6, IL-4, IL-8 and IL-13 in OE33R; radioresistant OAC cells. The secreted levels of 54 proteins in OE33P and OE33R cells was evaluated by multiplex ELISA, 30 proteins were detected in supernatant of OE33P and OE33R cells, 9 proteins were significantly upregulated in OE33R cells. Pyrazinib (P3) significantly inhibited the secretion of IL-6, IL-4, IL-8 and IL-13 in OE33R cells. Secreted levels of **(A)** Interleukin 6 (IL-6) **(B)** Interleukin 4 (IL-4) **(C)** Interleukin 8 (IL-8) **(D)** Interleukin 13 (IL-13) **(E)** Intracellular Adhesion Molecule 1 (ICAM-1) **(F)** Interleukin 12p70 (IL-12p70) **(G)** Interleukin 10 (IL-10) **(H)** Interleukin 2 (IL-2) **(I)** Interferon gamma-induced protein 10 (IP-10) **(J)** Monocyte chemoattractant protein 1 (MCP-1) in OE33P and OE33R cells treated with either 0.1% DMSO control or 10 µM pyrazinib (P3), all secretions normalised to protein content. Unpaired *t*-test used to compare different cell lines, paired *t*-test to compare within same cell line. (n = 3) *p < 0.05, **p < 0.01, ***p < 0.001. Data expressed as + SEM.

(P3) and P4, demonstrated greater anti-angiogenic activity than the quinoline series compound quininib, (Q1) in the ISV assay. Pyrazinib (P3) produced the most potent anti-angiogenic activity with a ~67% reduction in vessel number compared to control. The enhanced anti-angiogenic activity produced by pyrazinib (P3) and P4 of the P series was an important finding given that quininib, (Q1) a quinoline compound from which pyrazinib (P3) was derived has been previously shown to inhibit ocular and tumoural angiogenesis using *in-vitro* and *in-vivo* models and produces a potent anti-tumoural response in a colorectal murine xenograft model [29,30]. Thus, our initial findings indicated our novel small molecule compounds have more potent anti-angiogenic activity than quinoline series compound, quininib (Q1), and warrant further investigation in other model systems. The potent anti-angiogenic activity of our novel compounds is an important finding given that tumour vasculature has been recognised as a critical component of radiation response [12]. Aberrant tumour vasculature and dysregulated blood flow through tumour vasculature can promote the development of hypoxic regions which are associated with radioresistance [12]. Cells irradiated in the presence of oxygen are thought to be ~3 times more sensitive to irradiation than those located in regions of severe hypoxia [12]. In an oesophageal SCC xenograft model the administration of anti-angiogenic recombinant endostatin (rh-Endo) in combination with one dose of 8 Gy irradiation significantly delayed tumour growth which was associated with remodelling of the tumour vasculature and a reduction in tumour hypoxia in xenografts [16]. In a colon cancer xenograft model, an anti-VEGF monoclonal antibody in combination with radiation had an additive effect. The anti-VEGF antibody induced a significant tumour growth delay which was associated with a reduction in tumour microvessel density and interstitial fluid pressure [34]. These studies strongly support the development of a novel anti-angiogenic to enhance radiosensitivity. It is important to consider that the Tg*(fli1:*EGFP*)* zebrafish model used in this assay to identify our potent anti-angiogenic compounds is a model of developmental angiogenesis, and not pathological angiogenesis. Despite this, a large number of agents currently used in the clinic including sorafenib and regorafenib were previously shown to inhibit angiogenic activity in this zebrafish model [36]. In order to identify novel radiosensitisers with potential therapeutic benefit, it is likely that such agents will need to affect more than one biological process including metabolism to counteract the complex polymodal OAC radioresistant phenotype [11,33]. Thus, in addition to the anti-angiogenic activity produced by pyrazinib (P3) and other P series compounds, we investigated whether these compounds could also inhibit two major metabolic pathways, oxidative phosphorylation and glycolysis both *in-vivo* and *in-vitro* given the important association between oxidative phosphorylation and treatment response previously reported in OAC.

Zebrafish are becoming an increasingly popular model for cancer research and the use of this model for metabolic screening and profiling is continuing to emerge [37]. Pyrazinib (P3), P2 and P4 significantly reduced OCR, a measure of oxidative phosphorylation in zebrafish embryos, where pyrazinib (P3) and P2 produced a simultaneous reduction in ECAR, a measure of glycolysis. These findings suggest pyrazinib (P3) and P2 may be exerting their effect at an earlier point common to both metabolic pathways. Notably, Pyrazinib (P3) and P4, which were two of the most active compounds in both zebrafish assays have the same structural features including a (E)-2-(2-Pyridin-2-yl-vinyl)-phenol backbone but unlike pyrazinib (P3), P4 is a HCl salt, thus, the highly potent activity produced by P3 and P4 is likely to be attributable to these common structural features.

Additionally, *in-vitro*, pyrazinib (P3) and P2 produced a significant reduction in OCR a measure of oxidative phosphorylation of ~32% and ~18% respectively in OE33R (radioresistant) cells with pyrazinib (P3) producing a simultaneous reduction in ECAR, a measure of glycolysis. Notably, only pyrazinib (P3) produced significant anti-metabolic activity in both the OE33P and radioresistant OE33R cells. We have previously shown that OAC radio-resistant cells have an increased rate of oxidative phosphorylation when compared to radiosensitive OAC cells, thus, the potent inhibition of oxidative phosphorylation produced by our compounds is a significant finding in this model [11]. The higher rate of oxidative phosphorylation in OE33R radioresistant cells may indicate these cells consume more oxygen than radiosensitive cells and is thought to be a contributing factor promoting the radio-resistant phenotype given the importance of oxygen in the radioresponse, especially given that *ATP5B*, a marker of oxidative phosphorylation, is expressed at significantly higher levels in OAC patients with a subsequent poor response to neoCRT [11]. *In-vivo*, in HCT-116 xenografts,

administration of metformin was found to produce a 7% reduction in oxygen consumption rate and to improve tumour re-oxygenation [38]. In addition, in these xenografts, pre-treatment with metformin before one dose of 15 Gy irradiation produced a significant tumour growth delay [38]. Targeting oxidative phosphorylation *in-vivo* with papaverine was found to enhance tumour oxygenation an sensitise tumours to radiation therapy [39]. These studies highlight the potential of our novel anti-metabolic agents to enhance radiosensitivity, especially as pyrazinib (P3) can produce a much higher reduction in oxidative phosphorylation than metformin did in this study. ATP turnover was significantly higher in OE33R cells when compared to OE33P cells, supporting previous findings by our group [11]. Pyrazinib (P3) could significantly inhibit ATP turnover in OE33R cells. This is an important finding given that a previous study demonstrated that the maintenance of intracellular ATP levels following irradiation was associated with a radioresistant phenotype in head and neck cancer [40]. The ability of pyrazinib (P3) to reduce ATP turnover provides insight into how pyrazinib (P3) is significantly inhibiting oxidative phosphorylation in OE33R cells. The more potent anti-angiogenic and anti-metabolic activity produced by pyrazinib (P3) than its parent compound quininib may be attributable to their different structural features and molecular targets. Quininib, a quinoline compound, is a known cysteinyl leukotriene receptor 1 and receptor 2 antagonist whereas binding studies have shown that pyrazinib (P3), a pyrazine phenol does not target this molecular pathway [29]. Furthermore, previous studies have indicated that cancer cells can switch from a predominant glycolytic phenotype to an oxidative phenotype following radiation to promote cancer cell survival under genotoxic stress via mTOR-mediated hexokinase II inhibition [41] and p53-independent mitochondrial biogenesis, which is counter-regulated by HIF1α [42]. Thus, dual inhibition of both oxidative phosphorylation and glycolysis by pyrazinib (P3) in combination with anti-angiogenic activity is favourable. The lack of feedback upregulation of ECAR following OCR inhibition suggests pyrazinib (P3) is acting at an early point common to both pathways or there is a dysregulated compensatory mechanism in this isogenic model. In a pancreatic study inhibition of OCR with oligomycin was not found to cause an upregulation in ECAR [43]. Furthermore, metabolism is tightly linked to angiogenesis, as tumour vasculature supplies glucose to the tumour which is used to fuel the tricarboxylic acid cycle [44]. Thus the use agents targeting both angiogenesis and oxidative phosphorylation may be a novel approach that could be utilised to overcome radiation resistance.

In-vitro, OE33R cells were found to have significantly higher levels of ROS when compared to their matched OE33P cells which may be linked to the increased levels of mitochondrial mutagenesis in these cells [11]. The higher levels of ROS in the OE33R line may be a product of the extensive radiation exposure these cells underwent to become radioresistant but also highlights the altered mitochondrial function in radiation-resistant cells when compared to radiation-sensitive cells. Treatment with our novel compounds pyrazinib (P3), P2, P4, P18, P20, P8 and P23 significantly reduced ROS levels in the OE33P cells but no effect was seen in the treated OE33R cells. This inhibition of ROS specifically in our OE33P but not OE33R line was interesting and may indicate pyrazinib (P3) and other P series compounds (P2, P4, P18, P20, P8) can only alter inherently lower levels of ROS, as seen in OE33P cells, with no activity on the higher ROS levels in OE33R cells. Notably only pyrazinib (P3), which produced a reduction in ROS levels in OE33P cells, could also reduce oxidative phosphorylation in OE33P cells, potentially indicating that these compounds are targeting ROS generated from other processes outside the metabolic cycle, given no simultaneous reduction in metabolism is seen despite robust reductions in ROS produced by the other compounds. This result indicated that the previous reduction in metabolic rate by pyrazinib (P3) in OE33R cells is independent of changes to mitochondrial function and the reduction of either OCR or ECAR or both by pyrazinib (P3) and P2 is possibly occurring through an alternative mechanism. ROS is critical to the DNA damage response induced by irradiation, but on the contrary can promote cellular signalling and proliferation, thus a reduction of the higher levels of ROS in the OE33R cells following treatment may confer a favourable advantage [45]. In addition, this result indicates, the radiosensitising activity produced by pyrazinib (P3) is independent of changes to ROS in OE33R cells. Our results suggest that our P series compounds may be acting directly on these metabolic pathways, independent of significant changes to mitochondrial function.

Pyrazinib (P3) and P4, significantly enhanced radiosensitivity in both radiation-sensitive and radiation-resistant OAC cells. P2 could only enhance radiosensitivity in the radiation-sensitive OAC cells. Importantly, the quinoline compound quininib, (Q1) and the P series compounds which can inhibit angiogenesis but not OCR, a measure of oxidative phosphorylation could not enhance radioresponse. Furthermore, the enhanced radiosensitising effect was independent of changes to cellular proliferation or cellular cytotoxicity (Supplemental Fig. 1). These were significant findings which demonstrated that our lead small molecule compound; pyrazinib (P3), could enhance radiosensitivity in an isogenic model of OAC radioresistance as similar agents currently do not exist in this space. In addition, our lead compound, pyrazinib (P3), could also significantly enhance radiosensitivity when given before 4 and 6 Gy irradiation doses in both our OE33P and OE33R cells. Irradiation is a critical treatment modality which is used in the treatment of over 50% of human malignancies with response to radiation often inversely correlated to a reduction in tumour size [7]. This further highlights the importance of our identification of novel small molecule compounds which can enhance radiosensitivity in an isogenic model of OAC radioresistance. Importantly, clonogenic studies have been previously used to identify radiosensitising compounds *in-vitro* which have been later translated to radiosensitising agents in the clinic, an example of which is gemcitabine [46]. Thus, the clonogenic assay is a useful tool for the identification of potential novel radiosensitising agents, but it is important to note such assays lack the complexity of the heterogeneous tumour microenvironment. Furthermore, pyrazinib (P3) significantly enhanced radiosensitivity in OE33P and OE33R cells independent of baseline changes to the expression of DNA repair genes *MLH1*, *SMUG1*, *MMS19* and *PARP1* which have been previously linked to radiation resistance in OAC (Supplemental Fig. 3) [33].

Pre-treatment with pyrazinib (P3) could significantly enhance radiosensitivity of OE33R radioresistant cells following 4 Gy irradiation cultured under hypoxic conditions. Oxygen is a potent radiosensitiser and solid tumours with areas of hypoxia are the most aggressive and difficult tumours to treat [47]. Hypoxia is heterogeneous across tumours and can change following treatment radiation [48]. Hypoxic cancer cells are generally more resistant to both chemotherapy and radiotherapy than their normoxic counterparts and contribute largely to the development of treatment resistance and thus may serve as a novel target to enhance radiosensitivity. A number of studies have reportedly developed hypoxia-targeting agents as a mechanism to enhance radioresponse, thus the ability of pyrazinib (P3) to maintain its radiosensitising effect under these conditions is a critical finding. In gastric cancer, the RNA polymerase inhibitor TAS106 was demonstrated to radiosensitise gastric cancer cells and xenografts to irradiation through its action on HIF1α [49]. The ability of pyrazinib (P3) to radiosensitise OAC radioresistant cells under normoxic and hypoxic conditions further highlights the potential of this compound to function as a novel radiosensitiser in OAC.

OAC is an inflammatory driven cancer and we sought to investigate differences in inflammatory protein secretions in our isogenic model of OAC radioresistance. Nine of 30 detected inflammatory and angiogenic factors were secreted at significantly higher levels in OE33R radioresistant cells when compared to OE33P cells; IL-8, IL-4, IL-6, IL-2, IL-12p70, IL-10, MCP-1, IP-10 and ICAM highlighting the potential importance of these inflammatory and angiogenic mediators in radioresistance in OAC. Pyrazinib (P3) significantly reduced the secretions of IL-6, IL-8, IL-4 and IL-13 *in-vitro* in OE33R cells. Inflammation plays a

critical role in disease outcome in OAC, given the increased risk of cancer development and poor outcome for obese patients where altered secretion of adipokines and cytokines from adipose tissue contributes a pro-tumourigenic environment [50,51]. A previous study by our group showed a significant increase in oesophageal and colorectal tumour cell proliferation following culture with conditioned media from visceral adipose tissue of centrally obese patients which may be linked to the higher levels of IL-6 and VEGF found in this tissue [52]. IL-6 and its family members have been repeatedly linked with radioresistance of multiple tumour types including nasopharyngeal, liver, prostate, oral, and oesophageal cancer [25,53–57]. In a prostate cancer model, IL-6 inhibition enhanced radiosensitivity an effect which was associated with increased irradiation-induced ROS and oxidative DNA damage *in-vitro* and inhibition of IL-6 protein expression in combination with irradiation attenuated angiogenesis and decreased tumour regrowth *in-vivo* [55]. In addition, IL-6 signalling was reported to promote radioresistance through enhanced DNA repair and prevention of apoptosis in CD133+ stem-like cells of lung cancer after radiation [53]. Furthermore, IL-8 has also previously been linked with tumour radioresistance [58]. Let-7c, a tumour suppressor microRNA, was shown to restore radiosensitivity and impair stemness of oral cancer cells through inhibition IL-8 secretion [58]. In another study, in a radioresistant oral SCC xenograft, the administration of IL-8 and IL-6 neutralising antibodies sensitised the tumours to irradiation which supports our findings that inhibition of both IL-6 and IL-8 could contribute to enhanced radiosensitivity [27]. Similar to our findings, IL-6 and IL-8 were present at higher levels in radioresistant tumours when compared to the parental radiosensitive oral SCC tumours [27]. Furthermore, IL-4 and IL-13 are closely related cytokines which have also been previously linked with radioresistance, where the blockade of IL-4/IL-13 mediated phosphorylation of STAT6 produced a decrease in M2 polarization of macrophages and was protective against macrophage-mediated radioresistance of inflammatory breast cancer [59]. Given the association of IL-6, IL-8, IL-4 and IL-13 with tumour growth and treatment resistance in the literature, the inhibition of secretion of these cytokines by pyrazinib (P3) may further augment its anti-cancer effect. In summary, pyrazinib (P3), a novel anti-angiogenic and anti-metabolic compound, can significantly enhance radiosensitivity in an isogenic model of OAC radioresistance and is associated with anti-inflammatory activity through its inhibition of IL-6, IL-8, IL-4 and IL-13 secretion from OE33R cells.

Through phenotype-based drug discovery screens, we have identified pyrazinib (P3) as a novel radiosensitiser in OAC which produced robust anti-angiogenic and anti-metabolic activity *in-vivo* and *in-vitro* and significantly enhanced radiosensitivity in our isogenic model of OAC radioresistance under normoxic and hypoxic conditions. In addition, pyrazinib (P3) was shown to have significant anti-inflammatory activity through its inhibition of IL-6, IL-8, IL-4 and IL-13 inflammatory cytokine secretions. Importantly, *in-vitro* studies utilise tumour cells grown in a monolayer without the supporting stromal cells, endothelial cells and immune cells and it is possible the action of our compounds may be altered in the complex *in-vivo* tumour microenvironment. To further progress our studies, it will be critical to evaluate the effect of our lead radiosensitising compound, pyrazinib (P3), *ex-vivo* in human pre-treatment OAC biopsies and *in-vivo* in a murine model of OAC radioresistance to further elucidate its therapeutic potential in the future.

Author contributions

Experiments Designed by: AMB, BNK, JOS. Performed the experiments: AMB prepared all samples and performed all *in-vivo* and *in-vitro* assays, MRD ran multiplex ELISA. AC assisted in use of Seahorse Technology. SGM assisted with use of hypoxia chamber. ALR assisted in preparation of compounds. Analysed the data: AMB, SAK, NLL, JVR, BNK, JOS. Wrote the paper: AMB, BNK, JOS.

Conflicts of interest

No conflict of interest.

Funding

Funding for this work was provided by the Irish Cancer Society (Grant: CRS15BUC) and Health Research Board (Grant: HRB ILP-POR-2017-055), Enterprise Ireland Commercialisation Fund CF-2011-1319 awarded to BK supported the synthesis of the compounds.

Abbreviations

bFGF	Basic Fibroblast Growth Factor
DMSO	Dimethyl sulfoxide
Dpf	Days post fertilisation
ECAR	Extracellular Acidification Rate
EM	Embryo Medium
Hpf	Hours post fertilisation
IL-6	Interleukin 6
IL-4	Interleukin 4
IL-8	Interleukin 8
IL-13	Interleukin 13
ISV	Intersegmental Vessel
ICAM	Intracellular Adhesion Molecule 1
mTOR	Mammalian Target of Rapamycin
OAC	Oesophageal Adenocarcinoma
OCR	Oxidative Phosphorylation
NeoCRT	Neoadjuvant Chemoradiation Therapy
SCC	Squamous Cell Carcinoma
TRG	Tumour Regression Grade
RT	Room Temperature
VEGF-A	Vascular Endothelial Growth Factor A

Appendix A. Supplementary data

Supplementary data to this article can be found online at https://doi.org/10.1016/j.canlet.2019.01.009.

References

[1] J. Ferlay, et al., Cancer incidence and mortality worldwide: sources, methods and major patterns in GLOBOCAN 2012, Int. J. Canc. 136 (5) (2015) E359–E386.
[2] M. Arnold, et al., Global incidence of oesophageal cancer by histological subtype in 2012, Gut 64 (3) (2015) 381–387.
[3] A. Pennathur, et al., Oesophageal carcinoma, Lancet 381 (9864) (2013) 400–412.
[4] J. Cools-Lartigue, J. Spicer, L.E. Ferri, Current status of management of malignant disease: current management of esophageal cancer, J. Gastrointest. Surg. 19 (5) (2015) 964–972.
[5] T.N. Walsh, et al., A comparison of multimodal therapy and surgery for esophageal adenocarcinoma, N. Engl. J. Med. 335 (7) (1996) 462–467.
[6] H.-L. Jin, et al., Neoadjuvant chemoradiotherapy for resectable esophageal carcinoma: a meta-analysis, World J. Gastroenterol.: WJG 15 (47) (2009) 5983–5991.
[7] C.J. Lord, A. Ashworth, The DNA damage response and cancer therapy, Nature 481 (7381) (2012) 287–294.
[8] F. Pasini, et al., Neoadjuvant therapy with weekly docetaxel and cisplatin, 5-fluorouracil continuous infusion, and concurrent radiotherapy in patients with locally advanced esophageal cancer produced a high percentage of long-lasting pathological complete response, Cancer 119 (5) (2013) 939–945.
[9] C.L. Donohoe, J.V. Reynolds, Neoadjuvant treatment of locally advanced esophageal and junctional cancer: the evidence-base, current key questions and clinical trials, J. Thorac. Dis. 9 (Suppl 8) (2017) S697–S704.
[10] M. Westerterp, et al., Esophageal cancer: CT, endoscopic US, and FDG PET for assessment of response to neoadjuvant therapy—systematic review, Radiology 236 (3) (2005) 841–851.
[11] N. Lynam-Lennon, et al., Altered mitochondrial function and energy metabolism is associated with a radioresistant phenotype in oesophageal adenocarcinoma, PLoS One 9 (6) (2014) e100738.
[12] P. Wachsberger, R. Burd, A.P. Dicker, Tumor response to ionizing radiation combined with antiangiogenesis or vascular targeting agents: exploring mechanisms of interaction, Clin. Canc. Res. 9 (6) (2003) 1957–1971.
[13] W. Kim, et al., Inflammation-induced radioresistance is mediated by ROS-dependent inactivation of protein phosphatase 1 in non-small cell lung cancer cells,

Apoptosis 20 (9) (2015) 1242–1252.
[14] P.S. Ward, C.B. Thompson, Metabolic reprogramming: a cancer hallmark even warburg did not anticipate, Cancer Cell 21 (3) (2012) 297–308.
[15] O. Warburg, On the origin of cancer cells, Science 123 (3191) (1956) 309–314.
[16] H. Zhu, et al., Recombinant human endostatin enhances the radioresponse in esophageal squamous cell carcinoma by normalizing tumor vasculature and reducing hypoxia, Sci. Rep. 5 (2015) 14503.
[17] E. Ciric, G. Sersa, Radiotherapy in combination with vascular-targeted therapies, Radiol. Oncol. 44 (2) (2010) 67–78.
[18] B.A. Teicher, et al., Potentiation of cytotoxic cancer therapies by TNP-470 alone and with other anti-angiogenic agents, Int. J. Canc. 57 (6) (1994) 920–925.
[19] T. Hoang, et al., Enhancement of radiation response with bevacizumab, J. Exp. Clin. Canc. Res.: CR (Clim. Res.) 31 (1) (2012) 37-37.
[20] K.J. Williams, et al., Inhibition of vascular endothelial growth factor signalling using cediranib (RECENTINTM; AZD2171) enhances radiation response and causes substantial physiological changes in lung tumour xenografts, Br. J. Radiol. 81 (special_issue_1) (2008) S21–S27.
[21] B. Schmidt, et al., Combining bevacizumab with radiation or chemoradiation for solid tumors: a review of the scientific rationale, and clinical trials, Curr. Antimicrob. 1 (3) (2012) 169–179.
[22] H.J. Park, et al., Radiation-induced vascular damage in tumors: implications of vascular damage in ablative hypofractionated radiotherapy (SBRT and SRS), Radiat. Res. 177 (3) (2012) 311–327.
[23] S.G. Maher, et al., Serum proteomic profiling reveals that pretreatment complement protein levels are predictive of esophageal cancer patient response to neoadjuvant chemoradiation, Ann. Surg. 254 (5) (2011) 809–816 discussion 816-7.
[24] S.L. Picardo, et al., Barrett's to oesophageal cancer sequence: a model of inflammatory-driven upper gastrointestinal cancer, Dig. Surg. 29 (3) (2012) 251–260.
[25] S.-C. Liu, et al., Leukemia inhibitory factor promotes nasopharyngeal carcinoma progression and radioresistance, J. Clin. Invest. 123 (12) (2013) 5269–5283.
[26] A.M. Buckley, et al., Leukaemia inhibitory factor is associated with treatment resistance in oesophageal adenocarcinoma, Oncotarget 9 (72) (2018) 33634.
[27] E.V. Efimova, et al., Radioresistance of Stat1 over-expressing tumour cells is associated with suppressed apoptotic response to cytotoxic agents and increased IL6-IL8 signalling, Int. J. Radiat. Biol. 85 (5) (2009) 421–431.
[28] Z. Tahergorabi, M. Khazaei, The relationship between inflammatory markers, angiogenesis, and obesity, ARYA Atherosclerosis 9 (4) (2013) 247–253.
[29] A.G. Murphy, et al., Preclinical validation of the small molecule drug quininib as a novel therapeutic for colorectal cancer, Sci. Rep. 6 (2016) 34523.
[30] A.L. Reynolds, et al., Phenotype-based discovery of 2-[(E)-2-(Quinolin-2-yl)vinyl] phenol as a novel regulator of ocular angiogenesis, J. Biol. Chem. 291 (14) (2016) 7242–7255.
[31] Y. Alvarez, et al., Selective inhibition of retinal angiogenesis by targeting PI3 kinase, PLoS One 4 (11) (2009) e7867.
[32] C.B. Kimmel, et al., Stages of embryonic development of the zebrafish, Dev. Dynam. 203 (3) (1995) 253–310.
[33] N. Lynam-Lennon, et al., Alterations in DNA repair efficiency are involved in the radioresistance of esophageal adenocarcinoma, Radiat. Res. 174 (6) (2010) 703–711.
[34] C.G. Lee, et al., Anti-Vascular endothelial growth factor treatment augments tumor radiation response under normoxic or hypoxic conditions, Cancer Res. 60 (19) (2000) 5565–5570.
[35] N.A. Franken, et al., Clonogenic assay of cells in vitro, Nat. Protoc. 1 (5) (2006) 2315–2319.
[36] G. Chimote, et al., Comparison of effects of anti-angiogenic agents in the zebrafish efficacy–toxicity model for translational anti-angiogenic drug discovery, Drug Des. Dev. Ther. 8 (2014) 1107–1123.
[37] Y. Gibert, S.L. McGee, A.C. Ward, Metabolic profile analysis of zebrafish embryos, JoVE (71) (2013) e4300.
[38] C.W. Song, et al., Metformin kills and radiosensitizes cancer cells and preferentially kills cancer stem cells, Sci. Rep. 2 (2012) 362.
[39] M. Benej, et al., Papaverine and its derivatives radiosensitize solid tumors by inhibiting mitochondrial metabolism, Proc. Natl. Acad. Sci. Unit. States Am. 115 (42) (2018) 10756–10761.
[40] K. Goetze, et al., Glycolysis-related gene induction and ATP reduction during fractionated irradiation. Markers for radiation responsiveness of human tumor xenografts, Strahlenther. Onkol. 189 (9) (2013) 782–788.
[41] C.L. Lu, et al., Tumor cells switch to mitochondrial oxidative phosphorylation under radiation via mTOR-mediated hexokinase II inhibition–a Warburg-reversing effect, PLoS One 10 (3) (2015) e0121046.
[42] A. Bartoletti-Stella, et al., Gamma rays induce a p53-independent mitochondrial biogenesis that is counter-regulated by HIF1α, Cell Death Dis. 4 (6) (2013) e663.
[43] A. Viale, et al., Oncogene ablation-resistant pancreatic cancer cells depend on mitochondrial function, Nature 514 (7524) (2014) 628–632.
[44] M.G. Vander Heiden, L.C. Cantley, C.B. Thompson, Understanding the Warburg effect: the metabolic requirements of cell proliferation, Science 324 (5930) (2009) 1029–1033.
[45] S.S. Sabharwal, P.T. Schumacker, Mitochondrial ROS in cancer: initiators, amplifiers or an Achilles' heel? Nat. Rev. Canc. 14 (11) (2014) 709–721.
[46] T. Kausar, et al., Sensitization of pancreatic cancers to gemcitabine chemoradiation by WEE1 kinase inhibition depends on homologous recombination repair, Neoplasia 17 (10) (2015) 757–766.
[47] J.M. Brown, Exploiting the hypoxic cancer cell: mechanisms and therapeutic strategies, Mol. Med. Today 6 (4) (2000) 157–162.
[48] M.W. Dewhirst, Y. Cao, B. Moeller, Cycling hypoxia and free radicals regulate angiogenesis and radiotherapy response, Nat. Rev. Canc. 8 (6) (2008) 425–437.
[49] H. Yasui, et al., Inhibition of HIF-1alpha by the anticancer drug TAS106 enhances X-ray-induced apoptosis in vitro and in vivo, Br. J. Canc. 99 (9) (2008) 1442–1452.
[50] S.L. Doyle, et al., Visceral obesity, metabolic syndrome, insulin resistance and cancer, Proc. Nutr. Soc. 71 (1) (2012) 181–189.
[51] N. Ouchi, et al., Adipokines in inflammation and metabolic disease, Nat. Rev. Immunol. 11 (2) (2011) 85–97.
[52] J. Lysaght, et al., Pro-inflammatory and tumour proliferative properties of excess visceral adipose tissue, Cancer Lett. 312 (1) (2011) 62–72.
[53] Y. Chen, et al., IL-6 signaling promotes DNA repair and prevents apoptosis in CD133+ stem-like cells of lung cancer after radiation, Radiat. Oncol. 10 (2015) 227.
[54] M.F. Chen, et al., Role of interleukin-6 in the radiation response of liver tumors, Int. J. Radiat. Oncol. Biol. Phys. 84 (5) (2012) e621–e630.
[55] C.-T. Wu, et al., The role of IL-6 in the radiation response of prostate cancer, Radiat. Oncol. 8 (2013) 159-159.
[56] Y. Tamari, G. Kashino, H. Mori, Acquisition of radioresistance by IL-6 treatment is caused by suppression of oxidative stress derived from mitochondria after γ-irradiation, J. Radiat. Res. 58 (4) (2017) 412–420.
[57] Y. Matsuoka, et al., IL-6 controls resistance to radiation by suppressing oxidative stress via the Nrf2-antioxidant pathway in oral squamous cell carcinoma, Br. J. Canc. 115 (2016) 1234.
[58] C.Y. Peng, et al., Let-7c restores radiosensitivity and chemosensitivity and impairs stemness in oral cancer cells through inhibiting interleukin-8, J. Oral Pathol. Med. 47 (6) (2018) 590–597.
[59] O.M. Rahal, et al., Blocking interleukin (IL) 4-and IL13-mediated phosphorylation of STAT6 (Tyr641) decreases M2 polarization of macrophages and protects against macrophage-mediated radioresistance of inflammatory breast cancer, Int. J. Radiat. Oncol. Biol. Phys. 100 (4) (2018) 1034–1043.